Flexure of the continental lithosphere with multilayered rheology

E.B. Burov, Michel Diament

▶ **To cite this version:**

E.B. Burov, Michel Diament. Flexure of the continental lithosphere with multilayered rheology. Geophysical Journal International, 1991, 109 (2), pp.449-468. insu-01354127

HAL Id: insu-01354127

https://hal-insu.archives-ouvertes.fr/insu-01354127

Submitted on 17 Aug 2016

HAL is a multi-disciplinary open access archive for the deposit and dissemination of scientific research documents, whether they are published or not. The documents may come from teaching and research institutions in France or abroad, or from public or private research centers.

L'archive ouverte pluridisciplinaire **HAL**, est destinée au dépôt et à la diffusion de documents scientifiques de niveau recherche, publiés ou non, émanant des établissements d'enseignement et de recherche français ou étrangers, des laboratoires publics ou privés.

Geophys. J. Int. (1992) **109**, 449–468

Flexure of the continental lithosphere with multilayered rheology

E. B. Burov[1]* and M. Diament[2]

[1] *Institute of Physics of the Earth, Academy of Sciences of the USSR, B. Gruzinskaya* 10, *Moscow D-242, USSR*
[2] *Institut de Physique du Globe,* 4 *pl. Jussieu,* 75252 *Paris cedex* 05, *France*

Accepted 1991 November 26. Received 1991 November 26; in original form 1990 August 30

SUMMARY

In this paper, a model of flexure of the continental lithosphere is derived taking into account crustal and mantle rheologies. Bending of the continental lithosphere is modelled with a double yield stress envelope: three layers (brittle, elastic and ductile) for the crust and three analogous layers for the mantle portion. The deformation of the layers is controlled by the rheological properties of quartz-rich crustal rocks and olivine-rich mantle rocks. The influence of various factors such as the depth of Moho, strain rates, thermal structure of the lithosphere, boundary conditions, and topographic load, is examined. Results show that the mechanical strength of the continental lithosphere in the horizontal and vertical directions is primarily controlled by the present thermal structure of the plate, boundary forces and moments, and the applied topographic load. This explains why mountainous regions may be more locally compensated than adjacent regions. We also thus are able to explain why many continental plates have apparent effective rigidities much smaller than those predicted on the basis of their geological ages. The model is then applied to the Tien Shan–Tarim area (Central Asia), and original topography and gravity data are used to constrain parameters of the model. We found that the model satisfactorily matches the data and is also able to predict the thermal state of the plate and the location of the deep seismicity.

Key words: continental lithosphere, flexure, mechanical behaviour, rheology.

INTRODUCTION

Several authors have suggested various mechanical models of 2- or 3-D bending of oceanic and continental lithosphere (e.g. Watts & Talwani 1974; McNutt 1980; Karner & Watts 1983; Lyon-Caen & Molnar 1983, 1984; McAdoo & Sandwell 1985). In most continental cases the simplest model of local compensation (Airy isostasy), which neglects the horizontal stress redistribution due to flexure, does not satisfactorily explains the gravity signal, the seismic data and other geophysical observations (e.g. Dorman & Lewis 1972; Lyon-Caen & Molnar 1983, 1984).

To match the observations in areas where the local compensation model breaks down, it is essential to take into account stress redistribution due to flexure. Such mechanisms were introduced by applying different rheologies for the plate. These studies include elastic (e.g. Dubois *et al.* 1977; Karner & Watts 1983; Lyon-Caen & Molnar 1983), viscous (De Bremaecker 1977), viscoelastic (Melosh 1978) and elastic–plastic (McAdoo *et al.* 1978; Turcotte 1979) rheologies. Despite the fact that these models are characterized by more sophisticated rheologies and that for most purposes even a simple elastic model is good enough to fit the observations, there are still some problems to be solved, and one of the most important questions is: what can we learn about the real structure of the lithosphere and properties of lithospheric rocks from mechanical parameters obtained by fitting the model to the observations? In other words, do these parameters relate to available data on properties of rocks constituting the lithosphere as well as with the data on its structure? For example, in the case of purely elastic modelling the estimated 'effective' mechanical thickness of the lithosphere usually is smaller than the depth at which the rocks theoretically, can still preserve a quasi-elastic behaviour (McNutt, Diament & Kogan 1988). Another problem is that the effective thickness depends on the age, plate curvature, topographic load, and subduction angle (Kirby 1983; McNutt 1980; McNutt *et al.* 1988). The elastic plate model also predicts impossibly high stresses in the rocks which apparently may exceed the limit of yielding by several times (Goetze & Evans 1979; Lyon-Caen & Molnar 1983).

* Department of Earth Sciences, University of Leeds, Leeds LS2 9JT, UK.

Downloaded from http://gji.oxfordjournals.org/ at UPMC on August 16, 2016

More realistic models use data on mechanical properties of rocks, non-uniform layered lithospheric structure, the inferred thermal regime and other kinds of geophysical data. Models for layered rheology of the lithosphere account for non-uniform mechanical properties by introducing a three-layer (brittle–elastic–plastic) yield-stress envelope similar to that formulated by Goetze & Evans (1979) and McNutt & Menard (1982) and formerly applied almost exclusively to only the oceanic lithosphere (McAdoo, Martin & Polouse, 1985; Chamot-Rooke & Le Pichon 1989). The application of multilayered rheological models to the continental lithosphere is supported by the data of experimental rock mechanics (e.g., Brace & Kohlstedt 1980; Molnar & Tapponnier 1981; Kirby 1983, 1985; Kirby & Kronenberg 1987) which can be used for forward modelling. One can conclude from these investigations that the continental lithosphere differs mechanically from the oceanic one in that, for continents, a double (six-layer) yield stress envelope should be considered: three layers (brittle, elastic and ductile) for the crust and an analogous three layers for the mantle portion of the lithosphere. The use of rheological model with a double yield stress envelope for continents in place of the simpler oceanic envelope can be justified by several observations. First, continental crust is generally thicker (5–10 times) than the oceanic crust and therefore its contribution to the mechanical strength of the lithosphere cannot be neglected as is done in oceans. Consequently, as we cannot ignore the strength of the crust, we need to account for the significant difference between the mechanical properties of crustal and mantle rocks: it is generally assumed that low-temperature quartz creep dominates in the crust while in the mantle part high-temperature olivine creep prevails (Brace & Kohlstedt 1980). And, finally, the typical average radiogenic thermal productivity of the rocks of the continental crust (granites) is about of 10 times greater than that of the oceanic rocks (basalts) (Turcotte & Shubert 1982). As a result the radiogenic contribution to the total surface heat flux is 50 per cent or more. It significantly affects the position of the mechanical bottom of the crust (the depth below which yielding is geologically rapid) and, therefore, the total strength of the lithosphere. Depending on the stress regime and on the location of the mechanical bottom of the crust relative to the location of Moho, the crust can be mechanically coupled with or decoupled from the mantle part (Meissner & Strehlau 1982; Chen & Molnar 1983; Zoback, Prescott & Krueger 1985; McNutt *et al.* 1988).

In the present study we develop analytical and numerical methods to model the flexure of continental lithosphere using a realistic model for multilayered crustal and mantle rheologies. To test the model, data on gravity, topography and seismicity in the zone of convergence of the Tarim block and Kazakh shield (Central Asia) are used.

RHEOLOGICAL MODEL

Experimental and observational evidence indicates that rock fracture due to bending takes place at least to depths of 5–20 km (Brace & Kohlstedt 1980). As a result, frictional sliding develops on fractures until the yield stress is reached and brittle fracture of the whole volume of rock occurs. This process is relatively independent of temperature and can be described in terms of linear fracture mechanics (Byerlee 1968, 1978; Kirby 1983):

$$(\sigma_1 - \sigma_3) = 3.9\sigma_3 \quad \text{for } \sigma_3 \leq 120\ \text{MPa (depth less than 4–5 km)},$$

$$(\sigma_1 - \sigma_3) = 210 + 2.1\sigma_3 \quad \text{for } \sigma_3 \geq 120\ \text{MPa}, \tag{1}$$

where σ_1 and σ_3 are maximum and minimum principal stresses. The ductile behaviour of the crust is dominated by the creep of its main constituent (quartz) (Tsenn & Carter 1987). This mineral has a low temperature of creep activation, becoming weak at temperatures as low as 200 °C for stresses on the order of $\approx$0.5 MPa. At depths of about $h_1 = 25$ km corresponding to 350°–450 °C, quartz in the crustal part of the lithosphere has almost zero strength. Although crustal feldspar plays an important role, quartz is more ductile at lower temperatures and therefore the quartz creep law constrains the lower mechanical boundary of strength of the crustal rocks (Brace & Kohlstedt 1980). Kirby (1985) shows that other crustal rocks also have a critical temperature much lower than that for olivines. The rheological bottom of the crust (Moho) at depth h is also a mechanical discontinuity, since the sub-Moho olivine-rich rocks have a much higher temperature of ductile creep activation as compared to quartz-rich (granite, quartzite) crustal rocks (the strength of olivine is limited by the depth h_2 corresponding to a temperature of 700°–750 °C).

The upper part of the mantle portion of the lithosphere is also controlled by Byerlee's law (1) and by ductile behaviour which begins to play a part (for significant values of differential stress) starting from the depths corresponding to temperatures of $\approx$400°–600 °C. Regions between brittle and ductile zones of the plate preserve an quasi-elastic behaviour.

In general, the steady-state flow of both quartz and olivine can be described by the thermally activated power law with relevant parameters n, A, H^* (Kirby & Kronenberg 1987; Ranalli & Murphy 1987; Mackwell, Bai & Kohlstedt 1990):

$$\dot{\varepsilon} = A\,\Delta\sigma^n \exp(-H^*/RT) \tag{2}$$

$$\Delta\sigma = \left(\frac{\dot{\varepsilon}}{A}\right)^{1/n} \exp(H^*/nRT), \qquad H^* = E^* + PV^*, \tag{3}$$

where $\dot{\varepsilon}$ is the steady-state strain rate, $\Delta\sigma = (\sigma_1 - \sigma_3)$ is the differential stress, T is the temperature in Kelvin, A is a material constant, n ranges from 2 to 4.5 depending on the mineral, H^* is the activation enthalpy, E^* is the activation energy, P is the

Downloaded from http://gji.oxfordjournals.org/ at UPMC on August 16, 2016

hydrostatic pressure, and V^* is the activation volume. Following Goetze & Evans (1979), Brace & Kohlstedt (1980) and Molnar & Tapponnier (1981), we used an approximate form of (3) for dry olivine:

$$\Delta\sigma = \begin{cases} (\dot{\varepsilon}/A)^{1/n} \exp(E_1^*/nRT) & \text{for } \Delta\sigma \leqslant 200\,\text{MPa}, \quad (4a) \\ \sigma_0\left[1 - \left(\dfrac{RT \ln(\dot{\varepsilon}_0/\dot{\varepsilon})}{E_2^*}\right)^{1/2}\right] & \text{for } \Delta\sigma \geqslant 200\,\text{MPa}, \quad (4b) \end{cases}$$

where $n = 3$, $A = 7.0 \times 10^{-14}$, $E_1^* = 125$ kcal mol^{-1}, $E_2^* = 128$ kcal mol^{-1}, $\sigma_0 = 8.5 \times 10^9$ Pa, $\varepsilon_0 = 3.0 \times 10^{15}$ s^{-1}, and $R = 1.986$ cal (mol K)$^{-1}$. For quartz we use equation (4a) for $\Delta\sigma \leqslant 1000$ MPa with the following parameters: $n = 3$, $A = 5.0 \times 10^{-12}$, and $E_1^* = 45$ kcal mol^{-1} (Brace & Kohlstedt 1980).

For quasi-elastic portions of the plate we assume the Hookean behaviour

$$\sigma_{xx}(x, y) = \frac{E\varepsilon_{xx}(x, y)}{(1 - \vartheta^2)}, \quad (4c)$$

where E is the Young's modulus, $\vartheta = 0.25$ is the Poisson's ratio, and $\varepsilon_{xx}(x, y)$ is the horizontal strain at depth y with respect to the neutral plane.

The thermal structure of the lithosphere is better constrained for oceans than for continents, due to the high variability in concentrations of heat-producing elements in the continental crust (Sclater, Jaupart & Galson 1980; Turcotte & Shubert 1982; Kusznir & Karner 1985; De Rito *et al.* 1989). For this reason, the well-known half-space model of conductive cooling of the plate (Parsons & Sclater 1977) does not fit the geotherm based on metamorphic geothermometry data in the continental crustal areas (Sclater *et al.* 1980). We superimpose the radioactive heat flux q_r on the flux q_m due to conductive cooling of the plate to obtain the total heat flux $q(y) = q_r(y) + q_m(y)$ where $q_r = \rho_c H_s h_r \exp(-y/h_r)$; $H_s = 9.6 \times 10^{-10}$ W kg^{-1} is the heat production due to radiogenic decay, $h_r \approx 10$ km is the characteristic scale of a decrease in radiogenic heat production, and $\rho_c = 2670$ kg m^{-3} is the density of the crust (Sclater *et al.* 1980; Turcotte & Shubert 1982). To compute the geotherm, we solve the 1-D steady heat transfer equation (Carslaw & Jaeger 1964) using for $q(y)_m$ the expression for the heat flow through the mantle derived from (Parsons & Sclater 1977)

$$q_m(y) = -\frac{k_m T_m}{a}\left[1 + 2\sum_{n=1}^{\infty} \exp\left(\frac{-k_m \pi^2 t n^2}{\rho_m C a^2}\right) \cos\left(\frac{n\pi y}{a}\right)\right], \quad (5)$$

where $k_m = 3.35$ W (m K)$^{-1}$ is the thermal conductivity of mantle rocks, $T_m = 1350$ °C is the temperature at a depth $a = 250$ km which is taken as the thermal bottom of the lithosphere (Lerner-Lam & Jordan 1987, $\rho_m = 3300$ kg m^{-3} is the density of mantle rocks, $C = 10^3$ J kg^{-1} K^{-1} is the specific heat capacity of rocks, and t is the thermal age of the plate.

Assuming $q(0) = q_s = 60$ mW m^{-2}, $T(0) = T_s = 10$ °C, $q(h) = q_m(h) = Q_m$ and, for simplicity, $q(y) = q_r(y) + Q_m$ for the crust and $q(y) = q_m(y) + q_r(h)$, $q_r(h) \approx 0$ for the mantle, we can obtain an approximate solution for temperature distribution* in the continental lithosphere:

$$T(y, t) = \begin{cases} \dfrac{Q_m y}{k_c} + T_s + \dfrac{h_r(q_s - Q_m)[1 - \exp(-y/h_r)]}{k_c}, & y < h, \\ \dfrac{T_r(h - 0)(y - a)}{(h - a)} + T_m\left[\dfrac{y}{a} + \dfrac{2}{\pi}\sum_{n=1}^{\infty} \dfrac{\exp\left(\dfrac{-k_m \pi^2 t n^2}{\rho_m C a^2}\right) \sin\left(\dfrac{n\pi y}{a}\right)}{n}\right], & y \geqslant h. \end{cases} \quad (6)$$

In (6) we assume also that the radiogenic component of the temperature T_r is equal to zero at the depth $y = a$ since the shallow crustal radiogenic sources do not contribute to the thermal structure of the deep mantle. In any case, this contribution (no more than 100 °C) is not very important for deep mantle layers because of the much more important contribution (≈80 per cent) of the cooling component.

Using equations (4)–(6) we can compute the resulting yield-stress envelope for different values of strain rate $\dot{\varepsilon}$, Moho depth, and thermal age. The result is illustrated in Fig. 1 which shows the yield stress envelope for two different ages (175 and 500 Ma), and for a broad range of strain rates defining the onset of yielding in ductile regions. The value of h is fixed at 50 km. The calculation of the yield-stress envelope is primarily required by our mechanical model for the direct computation of the flexural deformations of the plate.

* We use the approximate solution because it is much simpler than the unwildly precise one (see the Appendix) and has a satisfactory accuracy of about 5–10 per cent.

Downloaded from http://gji.oxfordjournals.org/ at UPMC on August 16, 2016

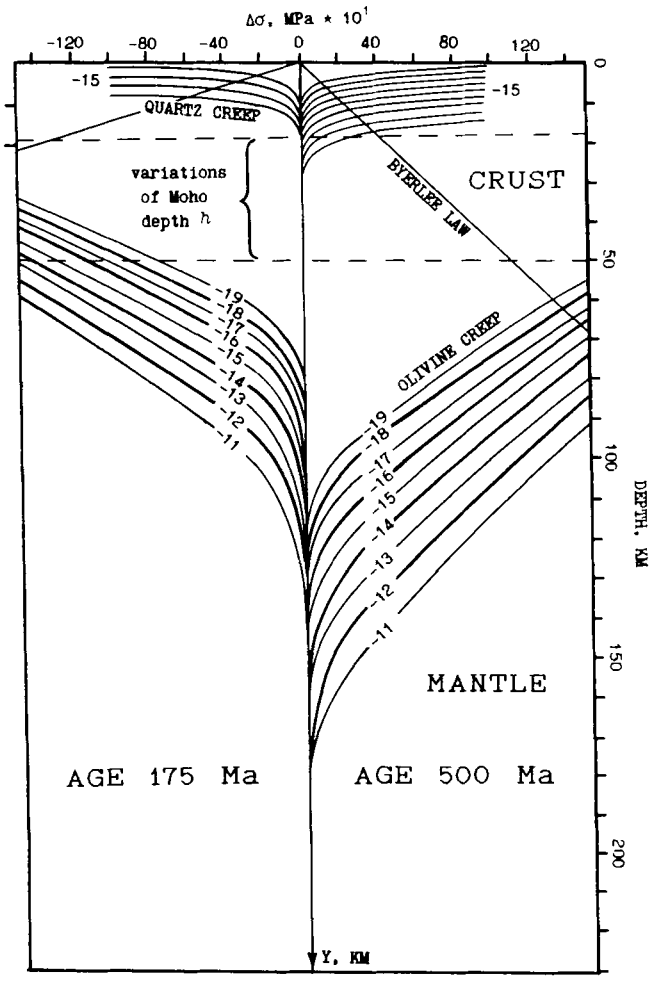

Figure 1. The yield-stress envelope resulting from expressions (4)–(6) for a broad range of strain rates $\dot{\varepsilon}$ defining the onset of yielding in ductile regions. The horizontal axis is differential stress, positive for tension and negative for compression. The vertical axis is depth, with positive downward. Dependent on Moho depth h and stress conditions, the gap between the mechanical bottom of the crust and the top of the mantle may be ductile or strong. The right side shows the tensional part of the envelope for the 500 Ma plate; the left side corresponds to the compressional part of the envelope for the 175 Ma plate. Curves marked $-11, -12, \ldots, -19$ correspond to $\dot{\varepsilon} = 1 \times 10^{-11}, 1 \times 10^{-12}, \ldots, 1 \times 10^{-19}\,s^{-1}$ respectively.

MECHANICAL MODEL

As seen in the previous section, stresses in the plate depend on temperature, on lithostatic pressure and curvature of the bending plate. Relations between these quantities are non-linear and consequently equations governing deformations of the plate will also be non-linear.

To model the bending of a lithospheric plate with non-linear behaviour of mechanical parameters, we consider the small 2-D dimensional (cylindrical) deflection $w(x)$ of a thin plate with non-linear rigidity $D(x, w'')$. In general, the relationship between the rigidity and $w(x)$ leads to appearance of terms containing derivatives of the rigidity with respect not only to x but also to $w(x)$ in the equation of the equilibrium of the plate. Nevertheless, the above assumption of small plate deflections allows one to neglect these terms as they are insignificantly small. Let $M = M(x, w_x'')$ be a non-linear bending moment acting on an elementary segment $(x, x + dx)$ of the plate. It is evident that a function $D(x, w'')$ exists such that

$$D(x, w_x'')\frac{\partial^2 w(x)}{\partial x^2} = -M(x, w_x'').$$

(For a linear case

$$D(x, w_x'') = D(x) = \frac{Eh_e^3(x)}{12(1-\vartheta^2)},$$

where $h_e(x)$ is the variable effective elastic thickness of the plate.)

Downloaded from http://gji.oxfordjournals.org/ at UPMC on August 16, 2016

The equilibrium state of the plate overlying an inviscid fluid and loaded by the laterally variable weight of the topography $P(x)$ is given by

$$-\frac{\partial^2 M}{\partial x^2}+\frac{\partial}{\partial x}\left(t(x)\frac{\partial w(x)}{\partial x}\right)+\Delta\rho(x)gw(x)=P(x), \tag{7}$$

where $t(x)$ is a net axial force, $\Delta\rho=\rho_m-\rho_s$ is the difference between the densities of underlying (mantle) and overlying material, and g is gravity.

We can rewrite (7) as a system of two equations:

$$\frac{\partial^2}{\partial x^2}\left(D(x, w_x'')\frac{\partial^2 w(x)}{\partial x^2}\right)+\frac{\partial}{\partial x}\left(t(x)\frac{\partial w(x)}{\partial x}\right)+\Delta\rho(x)gw(x)=P(x), \qquad D(x, w_x'')\frac{\partial^2 w(x)}{\partial x^2}=-M(x, w_x''). \tag{8}$$

For simplicity we assume that the horizontal force is constant: $t(x)=t(0)$.

The non-linear moment $M(x, w_x'')$ can be derived from (4)–(6) using

$$M(x, w_x'')=-\int_0^\infty \Delta\sigma(x, w_x'')y\,\partial y, \qquad t(x)=-\int_0^\infty \Delta\sigma(x, w_x'')\,\partial y. \tag{9}$$

In the quasi-elastic domains the stress is given by

$$\Delta\sigma=\sigma_{xx}(x, y)\approx-\frac{E}{(1-\vartheta^2)}\frac{\partial^2 w(x)}{\partial x^2}y^*=\gamma y^* \tag{10}$$

where $y^*=y-y_n$ is the distance from the depth y to the depth y_n which is the neutral plane, and

$$\gamma=-\frac{E}{(1-\vartheta^2)}\frac{\partial^2 w(x)}{\partial x^2}$$

is the gradient of the elastic deviatoric stresses.

The reasonable strain rate values may vary in the relatively broad range of 10^{-15}–$10^{-16}\,s^{-1}$ which corresponds, however, to almost the same geometry of the yield stress envelope (this is shown in Fig. 1). Molnar & Tapponnier (1981) used the value $\dot\varepsilon=3\times10^{-15}\,s^{-1}$ as most representative of the geological strain rate. We also chose the same value of $\dot\varepsilon$ to calculate the yield-stress envelope. At the next step, prior to inversion, we linearized the envelope by fitting segments of straight lines using least squares (Fig. 2). The flexural stress in the plate is then given by the following linear relations.*

Crust

Brittle regime (depths from 0 to $y1$ and from $y3$ to $y4$): $\Delta\sigma=\gamma_{b1}y$, $\gamma_{b1}=0.22\times10^5\,Pa\,m^{-1}$ for tension and $\gamma_{b1}=-0.66\times10^5\,Pa\,m^{-1}$ for compression.

Elastic regime (depths from $y1$ to $y2$):

$$\Delta\sigma=\gamma_c y_c^*=-\frac{E_1}{(1-\vartheta^2)}\frac{\partial^2 w(x)}{\partial x^2}(y-y_{n1}).$$

Ductile regime [depths from $y2$ to min (h_1, h)]:

$\Delta\sigma=\gamma_{d1}(y-h_1)$, $\gamma_{d1}=0.5$–$1.0\times10^5\,Pa\,m^{-1}$ for tension and $\gamma_{d1}=-|\gamma_{d1}|=-0.5$–$1.0\times10^5\,Pa\,m^{-1}$ for compression.

Mantle

Brittle/crust–mantle transition regime [depths from h to min $(y3, y4)$]:

$\Delta\sigma=\gamma_{b2}(y-h)$, $\gamma_{b2}=1.00\times10^{10}\,Pa\,m^{-1}$ for tension and $\gamma_{b2}=-1.00\times10^{10}\,Pa\,m^{-1}$ for compression; the area between the levels $h-y3$ appears only if some gradual transition from the crust to the mantle is considered. Because this transition is questionable, we treat the Moho as a discrete discontinuity by using a large value for γ_{b2}.

Elastic regime (depths from $y4$ to $y5$):

$$\Delta\sigma=\gamma_m y_m^*=-\frac{E_2}{(1-\vartheta^2)}\frac{\partial^2 w(x)}{\partial x^2}(y-y_{n2}).$$

Ductile regime (depths from $y5$ to h_2):

$\Delta\sigma=\gamma_{d2}(y-h_2)$, $\gamma_{d2}=0.231\times10^5\,Pa\,m^{-1}$ for tension and $\gamma_{d2}=-|\gamma_{d2}|=-0.231\times10^5\,Pa\,m^{-1}$ for compression.

* Throughout this paper, subscripts '1' and '2' refer to the crust and the mantle respectively.

Downloaded from http://gji.oxfordjournals.org/ at UPMC on August 16, 2016

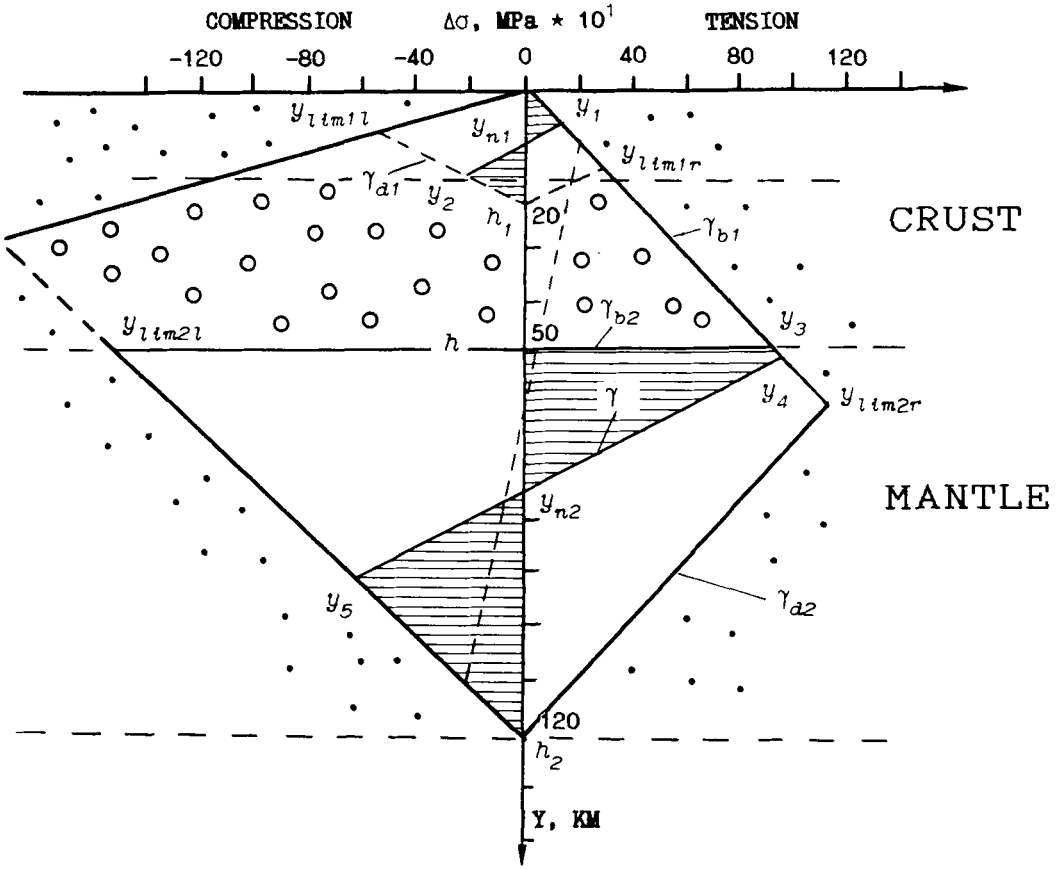

Figure 2. The linearized yield envelope used for numerical calculations. The dotted area marks the weak region. Open circles indicate the area which can be weak or not depending on the curvature and on the relative location of the Moho (with other parameters fixed). See text for further details.

E_1 and E_2 are the effective Young's moduli of the crustal and mantle lithosphere respectively. Although Young's modulus increases with depth, we use a constant value of 8.0×10^{10} N m^{-2} for both E_1 and E_2.

Assuming

$$t(x) = t = \frac{th_1}{h_1 + (h_2 - h)} + \frac{t(h_2 - h)}{h_1 + (h_2 - h)} = t_1 + t_2$$

and denoting $\Delta\sigma(y) = \sigma_{xx}(y) = \sigma(y)$, we finally obtain

$$\sigma(y) = \frac{t}{h_1 + (h_2 - h)} + \sigma_f(y, w'').$$

The term $\sigma_f(y, w'')$ on the right denotes the stress due to flexure. Although the presence of the net axial force t results in vertical shifts in the position of both neutral planes, we assume $t = 0$ in this study. Using (9), the depths of neutral planes in the crust and mantle are given by the following.

(a) In a case when $h_1 \geq h$ and the curvature of the plate is small enough [the elastic stress given by (10) is less than the yielding limit at the depth h], no decoupling will occur and the neutral plane will be at depth

$$y_n = \frac{h_2[1 + 2t/(|\gamma|D_2 h_2^2)]}{1 + \sqrt{1 + \left(\frac{B_1}{D_2} - 1\right)[1 + 2t/(|\gamma|D_2 h_2^2)]}}. \tag{11}$$

(b) Otherwise the plate is mechanically decoupled and two neutral planes are present at depths y_{n1} and y_{n2}:

$$y_{n1} = \frac{h_1[1 + 2(t_1 + S_1)/(|\gamma|D_1 h_1^2)}{1 + \sqrt{1 + \left(\frac{B_1}{D_1} - 1\right)[1 + 2(t_1 + S_1)/(|\gamma|D_1 h_1^2]}}. \tag{11a}$$

Downloaded from http://gji.oxfordjournals.org/ at UPMC on August 16, 2016

(c) If the elastic stress at the top of the mantle lithosphere is limited by Byerlee's law, y_{n2} is given by

$$y_{n2} = \frac{h_2[1 + 2(t_2 + S_2)/(|\gamma|D_2h_2^2)]}{1 + \sqrt{1 + \left(\frac{B_1}{D_2} - 1\right)[1 + 2(t_2 + S_2)/(|\gamma|D_2h_2^2)]}}. \tag{11b}$$

(d) At smaller curvature (see Fig. 1) the elastic core of the mantle is limited by the mechanical transition from the crust to the mantle and y_{n2} becomes

$$y_{n2} = \frac{h_2^*[1 + 2t_2/(|\gamma|D_2h_2^{*2})]}{1 + \sqrt{1 + \left(\frac{B_2}{D_2} - 1\right)[1 + 2t_2/(|\gamma|D_2h_2^{*2})]}}, \tag{11c}$$

where $B_i = |\gamma_{bi}/(\gamma - \gamma_{bi})|$, $D_i = |\gamma_{di}/(\gamma - \gamma_{di})|$, $h_2^* = h_2 - h$, $S_1 = -\gamma_{d1}(h_1 - h)^2/2$ if $h_1 \geqslant h$, otherwise $S_1 = 0$, and $S_2 = |\gamma_{b1}|\,h^2/2$.

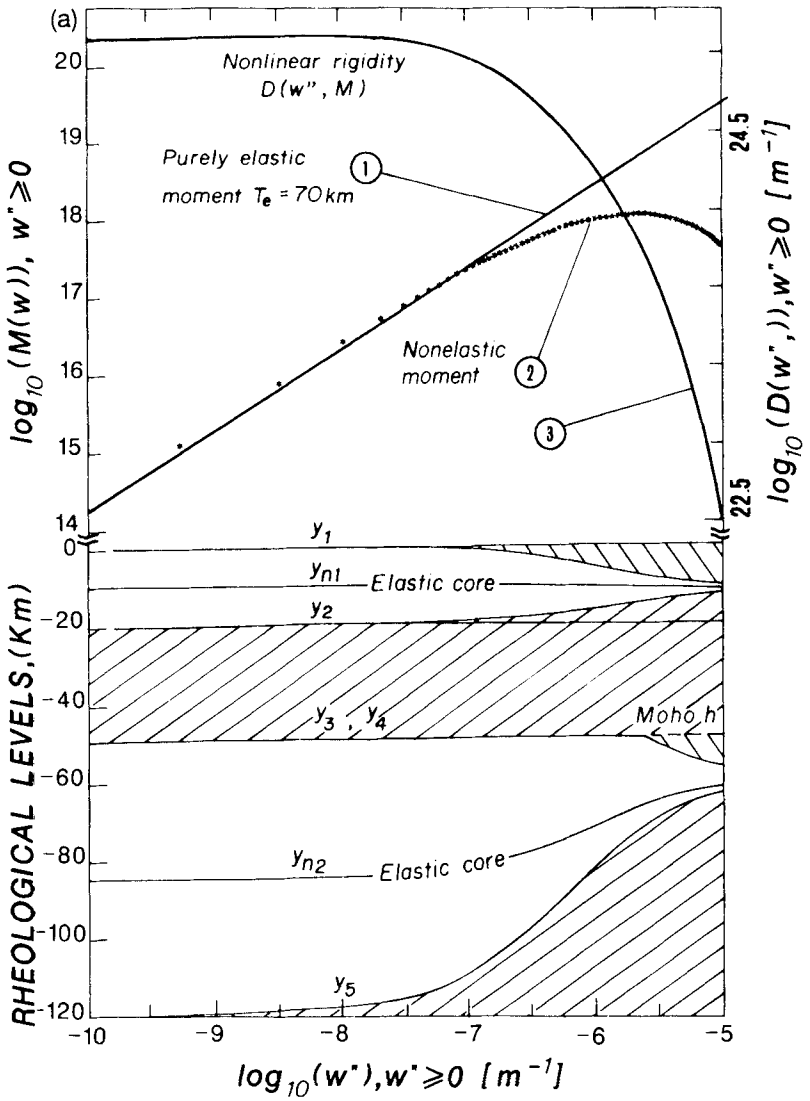

Figure 3. Dependence of the non-linear moment on the second derivative of the deflection w'' (w'' is inversely proportional to the radius of curvature) for $\geqslant$500 Ma plate with depth of mechanical bottom $h_2 = 120$ km and depth of Moho at 50 km (curve 2). The mechanical bottom of the crust is at depth $h_1 = 20$ km. Curve 1: purely elastic moment for an elastic plate with $h_e = 70$ km obtained from (12) for the same values of h_1, h_2 and h as for the non-elastic plate. Curve 3: effective rigidity corresponding to behaviour of non-linear moment. Behaviour of rheological layers is shown in the bottom. The areas corresponding to elastic cores of the crust and the mantle are within the boundaries y_1–y_2 and y_4–y_5 respectively. (a) Compression at the top, tension at the bottom ($w'' \geqslant 0$). (b) Tension at the top, compression at the bottom ($w'' \leqslant 0$). The plate is much weaker for concave upward flexure (when tensional failure prevails) than for the concave downward flexure (compressional failure prevails).

Downloaded from http://gji.oxfordjournals.org/ at UPMC on August 16, 2016

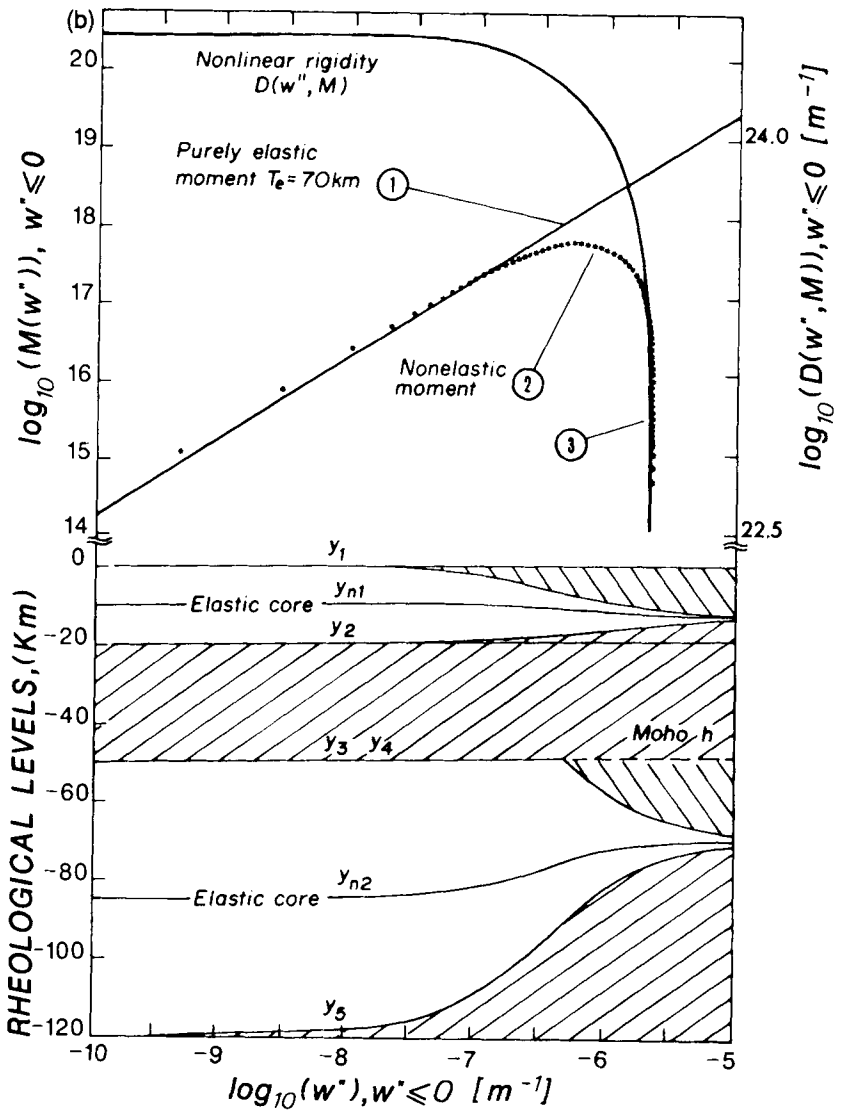

Figure 3 (*Continued*)

For $|\gamma| \leq 1$ (linear range of flexure, see Fig. 3) we assume

$$y_n = \tfrac{1}{2}h_2, \qquad y_{n1} = \tfrac{1}{2}h_1 \quad \text{and} \quad y_{n2} = \tfrac{1}{2}h_2^* + h.$$

Substitution of the above expressions for stress in (9) gives

$$M(x, w_x'') = \int_0^{y1} \gamma_1 y(y - y_{n1})\,\partial y + \int_{y1}^{y2} \gamma(y - y_{n1})^2\,\partial y + \int_{y2}^{\min(h_1, h)} \gamma_{b1} y(y - y_{n1})\,\partial y + \int_h^{y3} \gamma_{b2}(y - h)(y - y_{n2})\,\partial y$$

$$+ \int_{y3}^{y4} \gamma_{b1} y(y - y_{n2})\,\partial y + \int_{y4}^{y5} \gamma(y - y_{n2})^2\,\partial y + \int_{y5}^{h2} \gamma_{d2}(y - h_2)(y - y_{n2})\,\partial y.$$

Figure 3 shows the calculated moment for a broad range of admissible values of the curvature $-w''$ for an old plate ($t \geq 500$ Ma) with a depth of the mechanical bottom $h_2 = 120$ km and Moho depth at 50 km (parameters approximately corresponding to the Tarim basin, Central Asia). The corresponding behaviour of rheological layers is also given. Fig. 3 reveals that until some value of w'' is reached (about 10^{-7} m^{-1} in the given case), the bending moment has an almost linear 'elastic' behaviour. For larger values it becomes essentially non-linear and rapidly vanishes at a state of full 'saturation'. This situation corresponds to the appearance of a so-called 'plastic hinge' and occurs at larger values of stress for compression (Fig. 3a) than for the tension (Fig. 3b).

Downloaded from http://gji.oxfordjournals.org/ at UPMC on August 16, 2016

In the 'linear range' the moment for a plate with mechanically decoupled crust and mantle can be described as $M = -\gamma[h_1^3 + (h_2 - h)^3]/12$ which corresponds to a homogeneous plate with an effective elastic thickness h_e*:

$$h_e = [h_1^3 + (h_2 - h)^3]^{1/3}. \tag{12}$$

It is easy to see that $h_e \simeq \max(h_1, h_2 - h)$. For continents we generally have that $h_1 < h < h_2$, $(h_2 - h) \simeq 0.3h_2/0.5h_2 h_1 < (h_2 - h)$. The relation (12) thus explains the possibility of total reduction in the effective elastic thickness by a factor of 2 or more as compared to the non-decoupled (e.g. oceanic) plate with a maximum value of $h_e = h_2$. The maximum value of the effective elastic thickness of the continental crust is limited by a value of h_1 which is in general small enough compared to the maximum elastic thickness of the mantle part $h_2 - h$, whereas the 'spatial' thickness of the crust h (30–70 km) is about 30–60 per cent of the depth to the mechanical bottom of the lithosphere h_2 (90–130 km). It means that in spite of the presence of the thick crust the effective elastic thickness of the continental lithosphere is mainly controlled by the mechanical thickness of the mantle portion $h_2 - h$.

The typical proportions between the crustal and mantle parts in the continental areas are essentially different from that in the oceans: for the oceanic lithosphere the difference $h_2 - h$ is about $0.9h_2$ instead of $0.3h_2/0.5h_2$ for the continents (the thickness of the oceanic crust is ≈10 per cent of the total mechanical thickness). Since the crust is thin and the Moho boundary is shallow in the oceans, no decoupling with subsequent weakening occurs and the model with three rheological layers is enough to describe the flexure (Goetze & Evans 1979; McAdoo *et al.* 1985). As a result, the behaviour of an oceanic plate with mechanical thickness h_2 can be compared with the behaviour of approximately two times thicker ($\simeq 2h_2$) continental plate. This fact is illustrated in Fig. 4 which shows the deflection of an 80 Myr old oceanic plate (thermal thickness 125 km) with three-layer rheology (top of figure) and that of a 175 Myr old continental plate (bottom of figure) under similar boundary conditions. The figure shows that the thicker continental plate under the same conditions may be effectively even weaker than the oceanic one, due to the action of decoupling and due to the essential thermal weakening of the continental crust.

In order to solve the non-linear system (8), we apply an iterative approach using a finite difference approximation with linearization by Newton's method. In this approach the solution of the system of differential equations (8) is reduced to an iterative solution of a system of algebraic equations in a block matrix presentation. See details in Keller (1974) and Na (1979).

Substituting on the ith iteration $D(x, w'') = D_i(x)$, we used the same boundary conditions as in Burov *et al.* (1990):

(a) at infinity $(x \to \infty)$; $w(x) \to 0$, $dw(x)/dx \to 0$;

(b) at $x = 0$ for continuous plate we require

$$\left.\frac{dw(x)}{dx}\right|_{x=0} = 0, \qquad \left.\frac{d}{dx}\left(D_i(x)\frac{d^2w(x)}{dx^2}\right)\right|_{x=0} = 0;$$

(c) at $x = 0$ for a broken plate we have

$$M(0) = -D_i(x)\frac{d^2w(x)}{dx^2}, \qquad \left.\frac{d}{dx}\left(D_i(x)\frac{d^2w(x)}{dx^2}\right)\right|_0 = F(0) + t(0)\left.\frac{dw(x)}{dx}\right|_0,$$

where $F(0)$ and $M(0)$ are respectively a boundary vertical shear force and a boundary moment per unit length applied to the end of the plate.

Since many continental thrust belts are the result of ancient plate collisions and are at present seismically inactive, there are difficulties with visualizing the slab geometry. This is in contrast to the oceanic subduction zones where the seismic data closely constrain plate geometry. The upper surface of the deflected continental plate also cannot be observed in the topography, being partly masked by sediments, erosion, and tectonic processes which alter the surface topography. Therefore gravity data appear to be one of the most reliable quantitative constraints on the model. To compute a theoretical gravity signal due to the deformation of density boundaries caused by the deflection of the plate, we calculated gravity anomalies produced by semi-infinite polygonal blocks (with densities of sediments, crust and mantle), the geometry of which is defined by the solutions for deflection (Talwani, Worzel & Landisman 1959). The theoretical gravity signal is then compared with observed gravity anomalies.

To obtain the deformation of the structural layers of the plate, we vary the same number of parameters as in pure elastic modelling, but vary the thermal age instead of the flexural rigidity. Since the thermal age of the plate can be deduced from the geological age and other data, it is even a better constrained parameter than the effective rigidity. All other parameters (strain rate, material constants, activation energy and thermal thickness of the lithosphere) are taken from experimental data and are held constant. Although we do not vary most parameters in the model, it is important to understand how uncertainties in the estimation of these parameters affect our results. The strain rate may vary up to an order of magnitude from the value used

* Throughout this paper the term 'effective elastic thickness', if applied to the plate with non-linear rheology, is generally related to the 'linear range' described by (12).

Downloaded from http://gji.oxfordjournals.org/ at UPMC on August 16, 2016

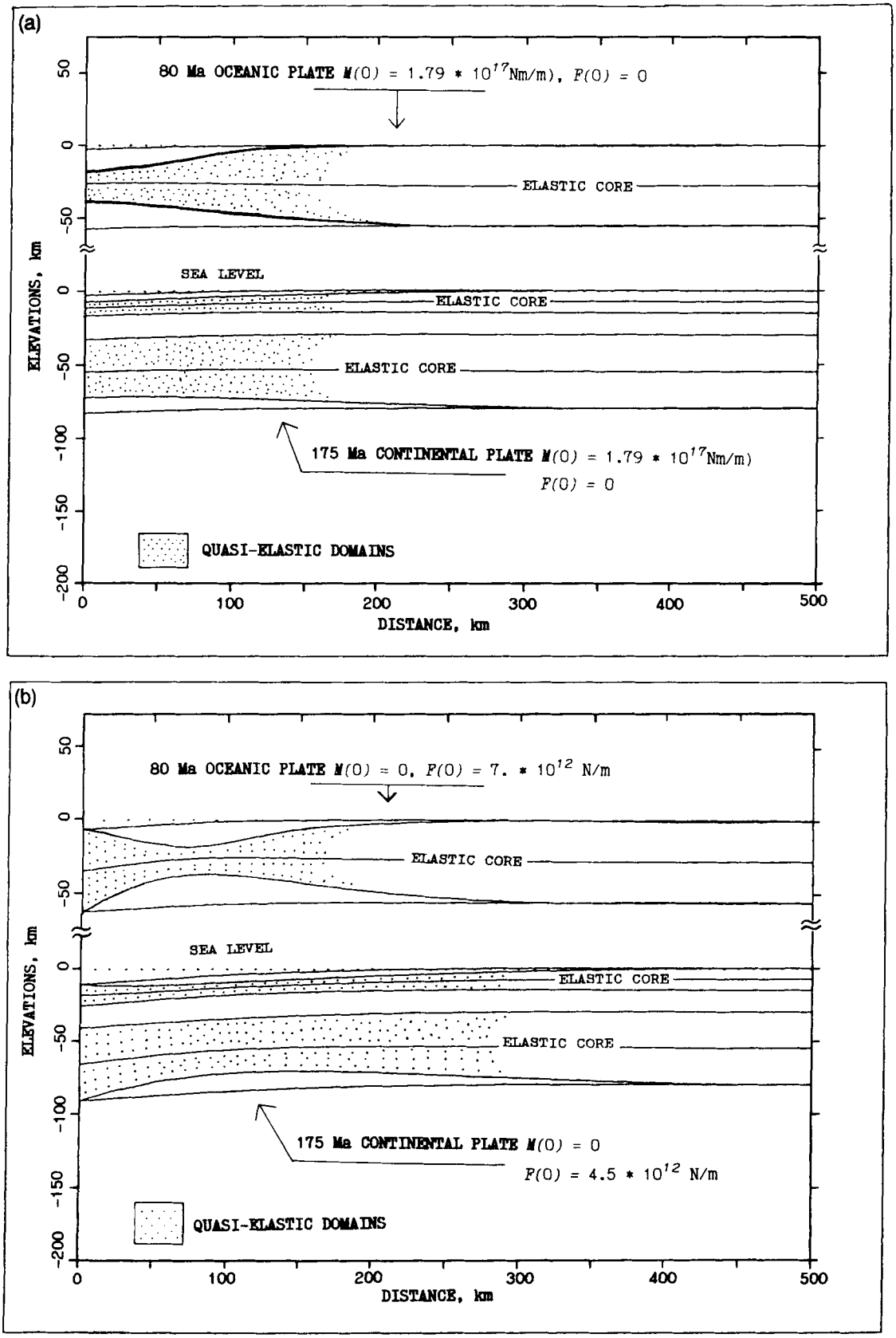

Figure 4. Deflection of a three-layer 80 Ma oceanic plate (thermal thickness 125 km, mechanical thickness 57 km, $\gamma_{d2} = 40\,000$ Pa m^{-1}) (McAdoo *et al.* 1985), compared with the deflection of the young 175 Ma continental plate ($h_1 = 15$ km, $h = 30$ km, $h_2 = 80$ km, $\gamma_{d1} = 125\,000$ Pa m^{-1}, $\gamma_{d2} = 40\,000$ Pa m^{-1}, see also Fig. 1). Identical boundary conditions are imposed for each case. (a) Non-zero boundary moment $M = 1.79 \times 10^{17}$ N mm^{-1}, zero force $F = 0$. (b) Zero moment, non-zero boundary force $F = 7.0 \times 10^{12}$ N m^{-1} for oceanic plate and 4.5×10^{12} N m^{-1} for the continental one. (c) Non-zero moment and force: $M = 1 \times 10^{17}$ N mm^{-1}, $F = 2 \times 10^{12}$ N m^{-1}.

Downloaded from http://gji.oxfordjournals.org/ at UPMC on August 16, 2016

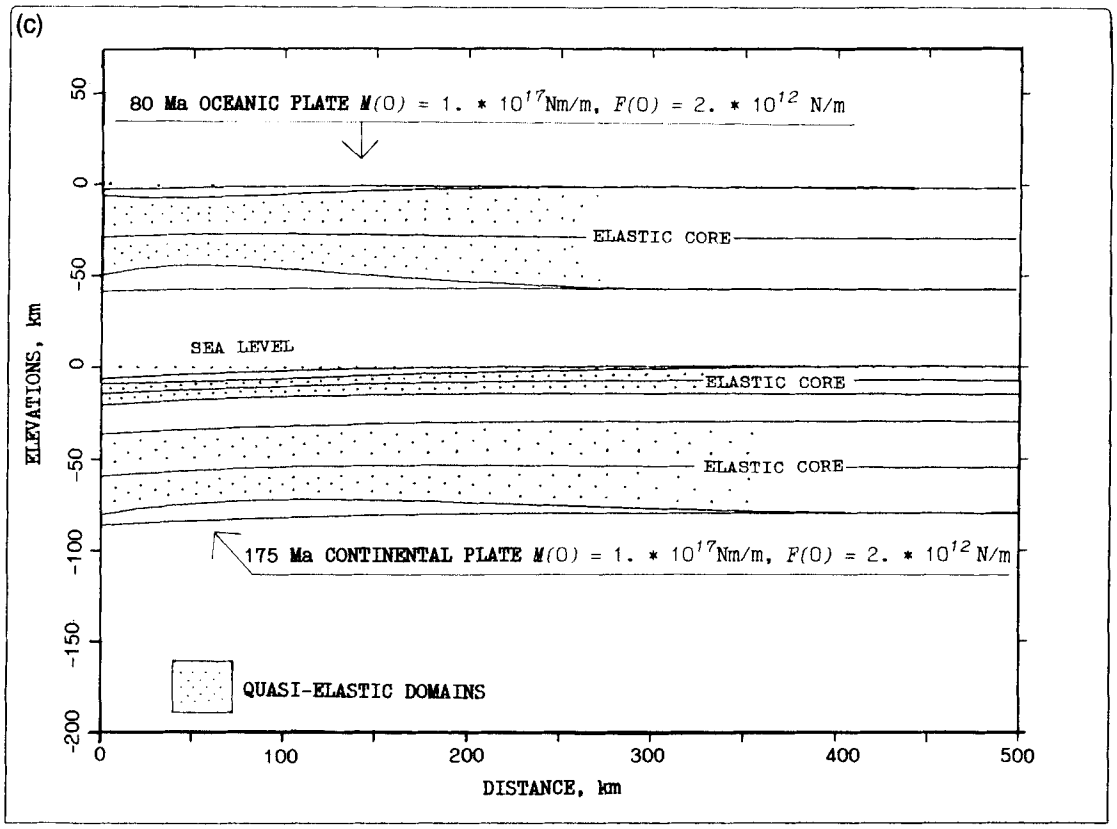

Figure 4 (*Continued*)

here, but such a variation has little effect on the slope of the yield envelope and alters the depth to the mechanical bottom of the plate by less than 10 per cent (see Fig. 1). The effect of errors in other parameters is of comparable order, but it becomes smaller: as the age of the plate increases, the non-equilibrium components of the lithospheric temperature structure decay exponentially with time, and the geotherm approaches a linear conductive gradient. As a result, the yield envelope remains approximately the same for ages greater than 500–1000 Myr within the uncertainty of parameters in equations (4a)–(4b). Uncertainties in the parameters are not very important especially if the plate is thermally older than 400–500 Myr which is a common case for many continental regions.

RESULTS AND DISCUSSION

As we could see, the average strength of the lithosphere depends on the parameters of the yield stress envelope accounting for rheological and thermal structure of the lithosphere. The horizontal variations of the strength depend on various local conditions including the boundary moments and forces, the distribution of outer loads and horizontal inhomogeneities in the thermal and rheological structure of the lithosphere. The last two factors result in local variations in the shape of the yield-stress envelope.

Let the general shape of the yield-stress envelope be fixed. In this case we can independently examine the influence of the boundary conditions and outer loads on the flexural deformations of the plate and, consequently, on its effective strength and the internal structure. The relation between the local radius of curvature and the value of the bending moment was already shown in Fig. 3. The behaviour of a continental plate with typical parameters under various boundary conditions is illustrated in Fig. 5. Figs 3 and 5 show that, having reached some limiting value, both boundary moments and forces can create a significant zone of plate thinning and a subsequent loss of effective rigidity. The size of this zone depends on the initial mechanical thickness of layers and on the curvature. The plate may lose more than half of its initial thickness near the point of maximum value of $|w''|$. Due to the significant asymmetry of the envelope, the problem becomes undetermined well before the upper and lower boundaries of elastic layers join each other. The location of the weak zone depends on the specific boundary conditions and on the loads applied to the plate. It is important to take this fact into account if some observational data on flexure are used to estimate an average effective rigidity or strength of the plate.

The main difference in the effect of boundary moments and of forces is that the moment produces maximum thinning almost immediately at the edge of the plate, while the force creates thinning somewhere in the middle, between the edge and

Downloaded from http://gji.oxfordjournals.org/ at UPMC on August 16, 2016

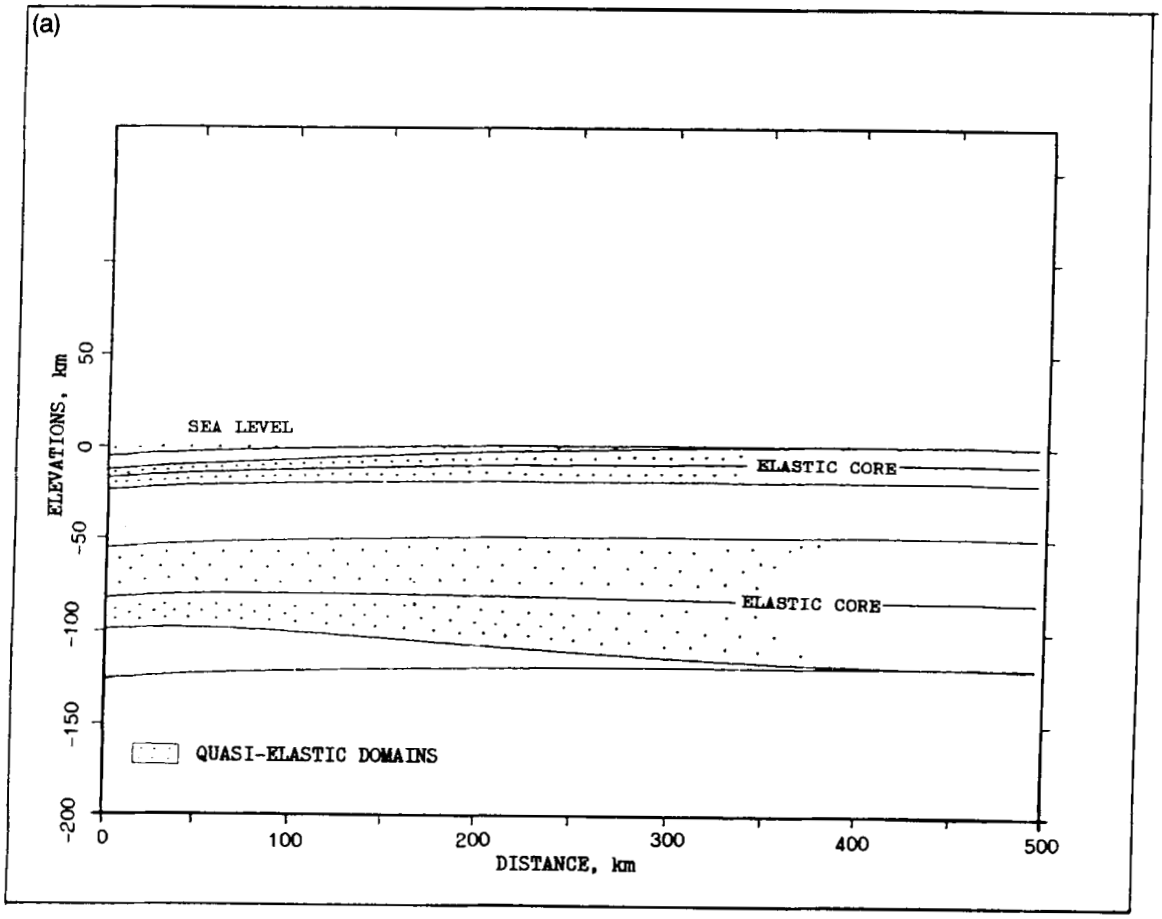

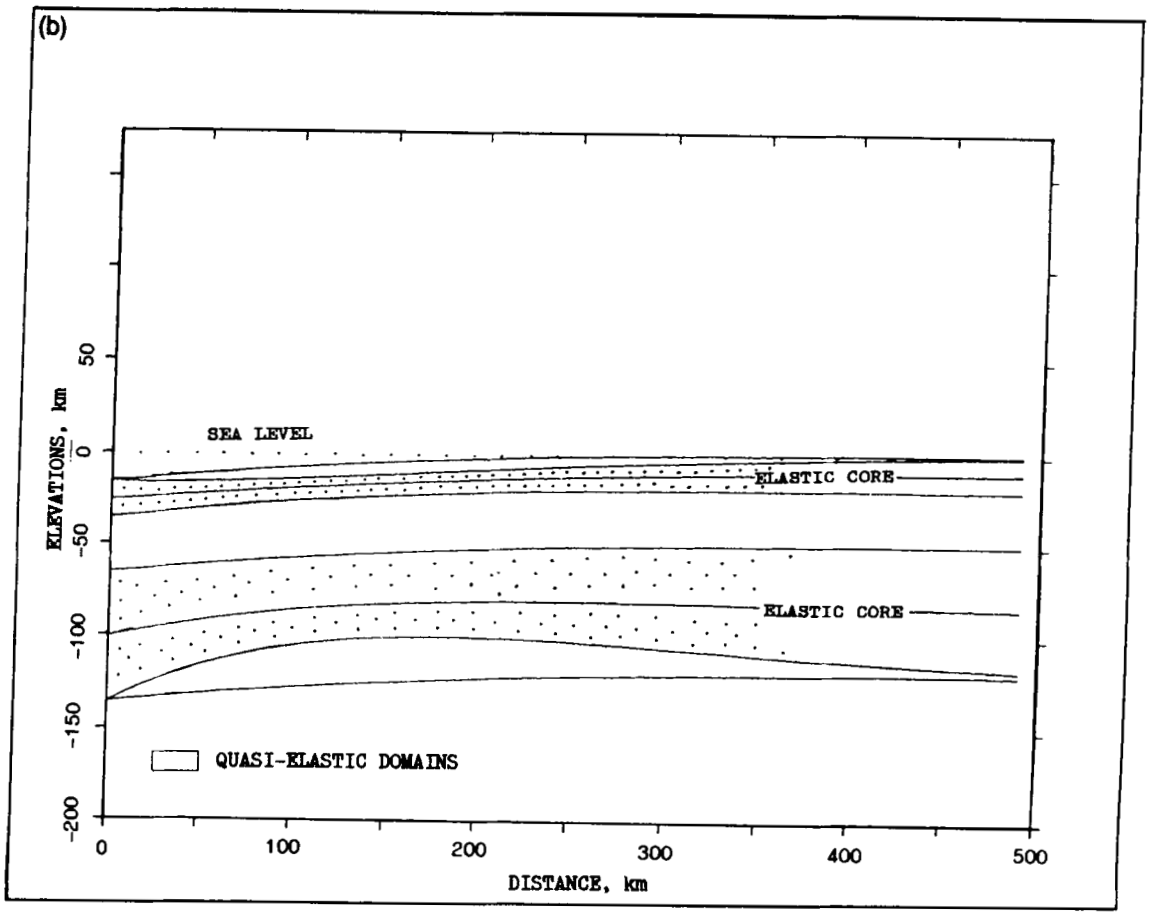

Figure 5. Behaviour of an old (≈500 Ma) continental plate assuming parameters close to these of the Tarim Block (Central Asia). (a) $M = 5.0 \times 10^{17}$ N m m^{-1}, $F = 0$. (b) $M = 0.0$, $F = 8.0 \times 10^{12}$ N m^{-1}. (c) $M = 5.0 \times 10^{17}$ N m m^{-1}, $F = 5.0 \times 10^{12}$ N m^{-1}. (d) $M = 5.0 \times 10^{17}$ N m m^{-1}, $F = 8.0 \times 10^{12}$ N m^{-1}.

Downloaded from http://gji.oxfordjournals.org/ at UPMC on August 16, 2016

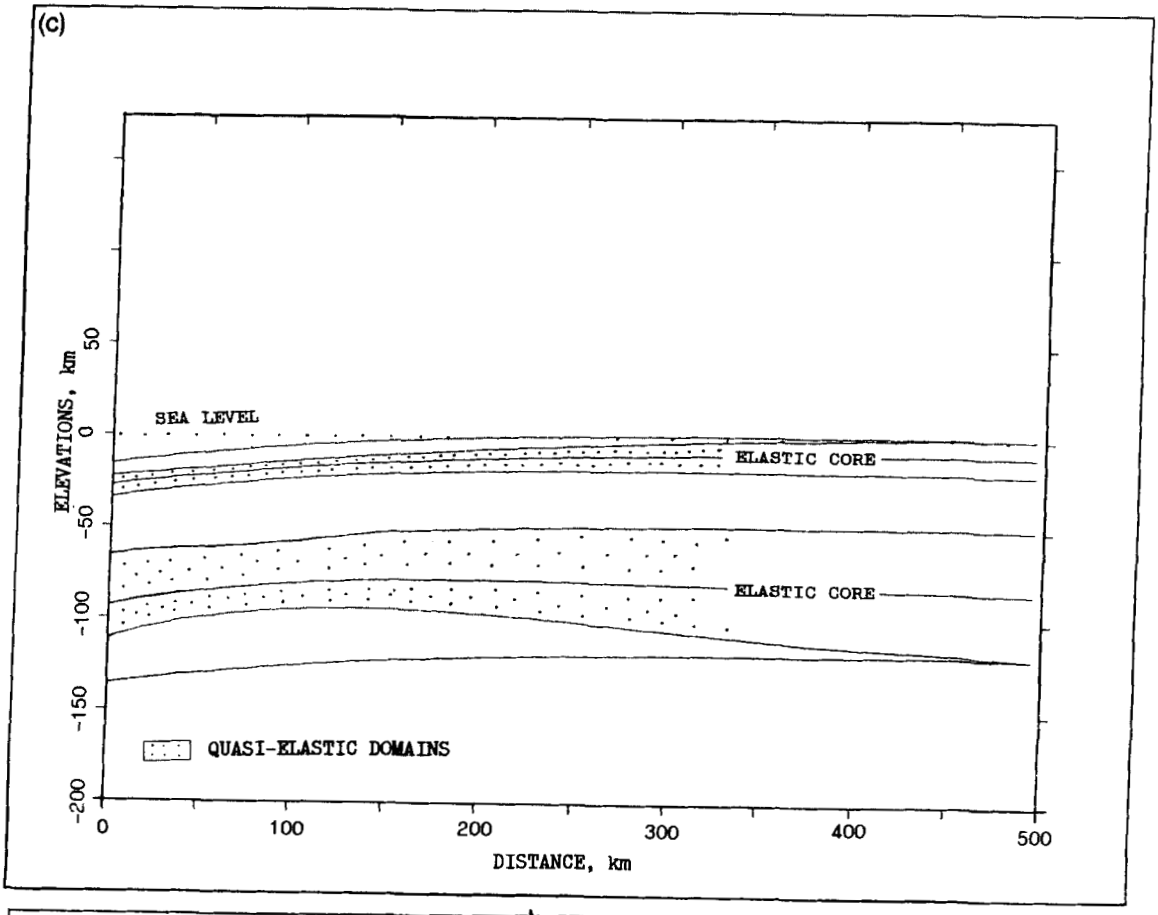

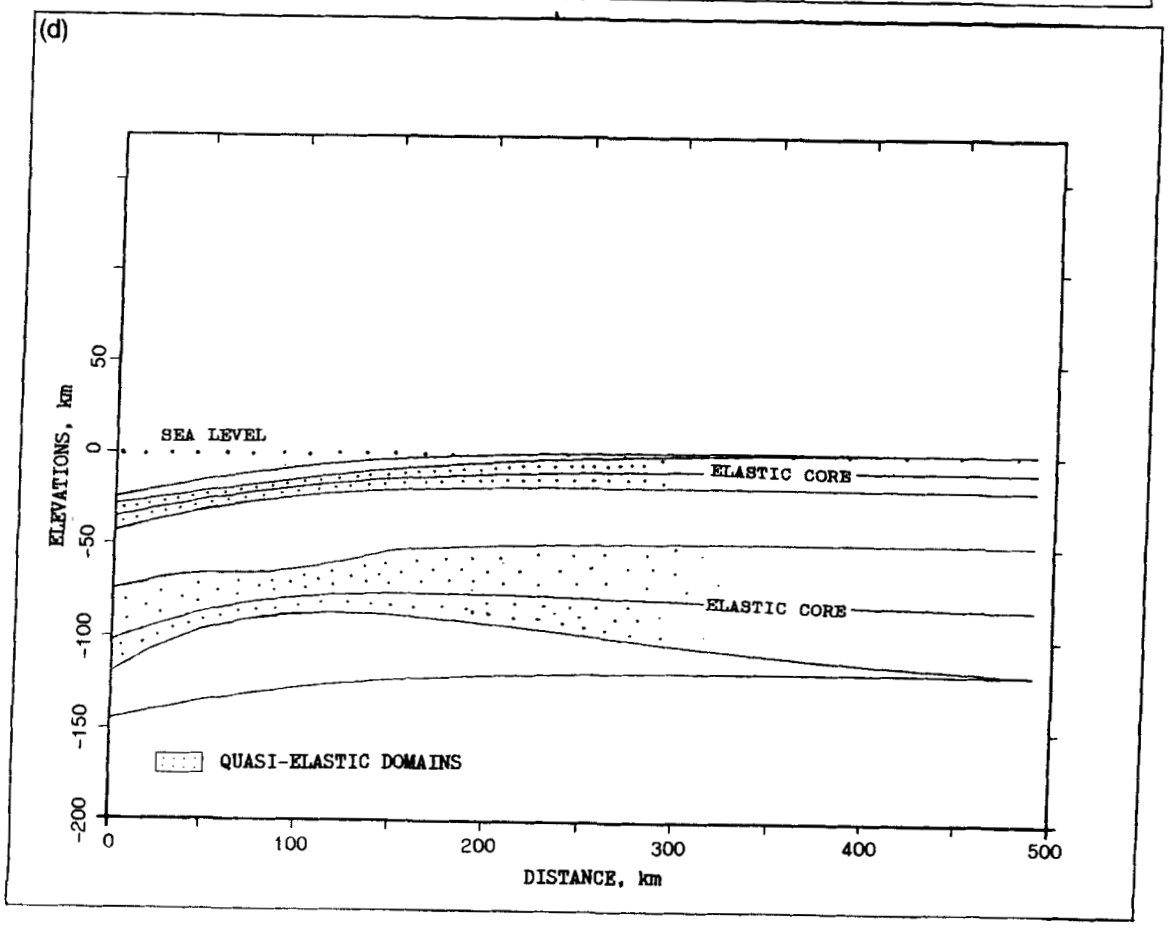

Figure 5 (*Continued*)

Downloaded from http://gji.oxfordjournals.org/ at UPMC on August 16, 2016

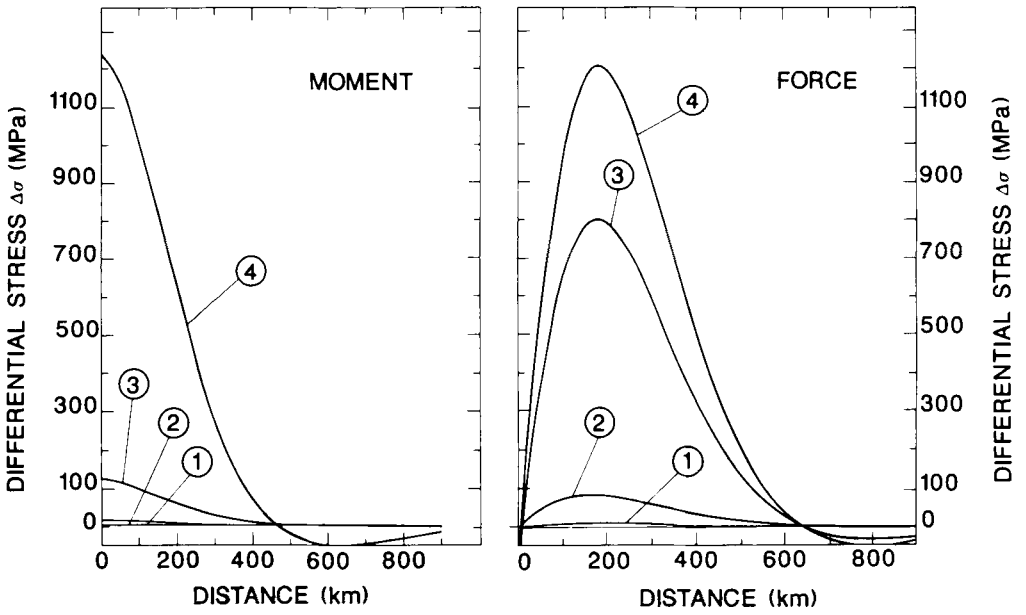

Figure 6. Stress distribution for a simple purely elastic plate with equivalent elastic thickness $h_e = 70$ km: comparison of the effect of the boundary moment and force. The moment produces maximum thinning almost immediately at the edge of the plate while the force does the same somewhere in the middle between the edge and the peripheral uprise. The larger the force, the closer is the area of the minimal thickness to the edge of the plate. Moment (left-hand side): curve 1, $M = 1.0 \times 10^{15}$ N m m^{-1}; curve 2, $M = 1.0 \times 10^{16}$ N m m^{-1}; curve 3, $M = 1.0 \times 10^{17}$ N m m^{-1}; curve 4, $M = 1.0 \times 10^{18}$ N m m^{-1}. Force (right-hand side): curve 1, $F = 1.0 \times 10^{11}$ N m^{-1}; curve 2, $F = 1.0 \times 10^{12}$ N m^{-1}; curve 3, $F = 1.0 \times 10^{13}$ N m^{-1}; curve 4, $F = 1.5 \times 10^{13}$ N m^{-1}.

the flexural bulge. It can be explained by an example of stress distribution in a simple purely elastic plate with effective thickness $h_e = 70$ km (Fig. 6). The larger the force, the closer the area of the minimal thickness is to the edge of the plate. The force also affects the position and amplitude of the flexural bulge. A decrease in thickness attenuates the horizontal propagation of stress and results in the elastic unloading of the plate outside the weak zone.

Distributed topographic loads have an effect similar to that of boundary forces and moments. Indeed, Fig. 7 demonstrates the appearance of a remarkably weakened zone beneath a mountain load ('Gaussian' mountain 5 km in height, radius 100 km). In the given example the effective rigidity of the plate (with parameters same as in Fig. 4) becomes almost two times thinner below the most loaded area. The manifestation of this effect in the gravity field is shown by a comparison of gravity anomalies computed using the non-linear rheology ($h_1 = 15$ km, $h = 30$ km, $h_2 = 80$ km) and the purely elastic case $h_e = [h_1^3 + (h_2 - h)^3]^{1/3} \approx 50$ km. It follows from this example that the plates may be weaker and therefore may appear more 'locally compensated' beneath mountainous regions than in adjacent areas. This effect is especially important when the region is thermally young, in regions where the Moho is deep compared to the depth of the mechanical boundary layer in the mantle lithosphere, or in areas where the heat flux through the mantle is significantly larger than the heat flux due to cooling only. For example, for areas where $q_s = 90$–200 mW m^{-2}, the additional contribution to the temperature–depth law (6) will be 15°–40 °C km^{-1}. This may shift the mechanical boundary upward by up to tens of kilometres and decrease the mechanical thickness of the plate beneath the load *several* times. Increased heat flux causes thermal weakening of the lithosphere and reduces the apparent flexural rigidity. As a result the rigidity of the crust may become negligible. It is clear from comparison with action of the boundary force that, if the load is highly asymmetric, the area of the maximum thinning is not necessarily beneath the point of a maximum load.

Finally, to examine the applicability of our model, we tested our approach on the case of Tarim block and Kazakh shield which collide beneath the Central and Eastern Tien Shan (Central Asia). The topography and gravity data profiles used here were published and discussed earlier in Burov *et al.* (1990). We just briefly recall some geodynamical considerations. The area represents a zone of interaction between the Precambrian Tarim block which advances from the south and the Kazakh shield which moves from the north (Fig. 8). Bouguer gravity anomalies over the Tien Shan in this area are within about 50 mgal of those expected for local Airy compensation and require an additional support of an uncompensated mass deficit. Assuming a purely elastic model, Burov *et al.* (1990) found that both colliding plates (of approximately the same geological age) subduct almost symmetrically beneath the Tien Shan. Furthermore, the equivalent flexural rigidity of the northern plate appeared to be very small ($h_e \simeq 15$–25 km, $D < 10^{23}$ N m), especially in comparison with that of the southern plate ($h_e \simeq 50$–60 km, $D \simeq 10^{24}$ N m). It was also shown that a significant value of the boundary force (1–5×10^{12} N m^{-1}) and/or moment ($\simeq 2 \times 10^{16}$ N m^{-1}) per unit length was required to fit the gravity data. In addition, Burov & Kogan (1990) detected a preference of approximately 30 per cent thinning at the subducting edges of the plates.

Downloaded from http://gji.oxfordjournals.org/ at UPMC on August 16, 2016

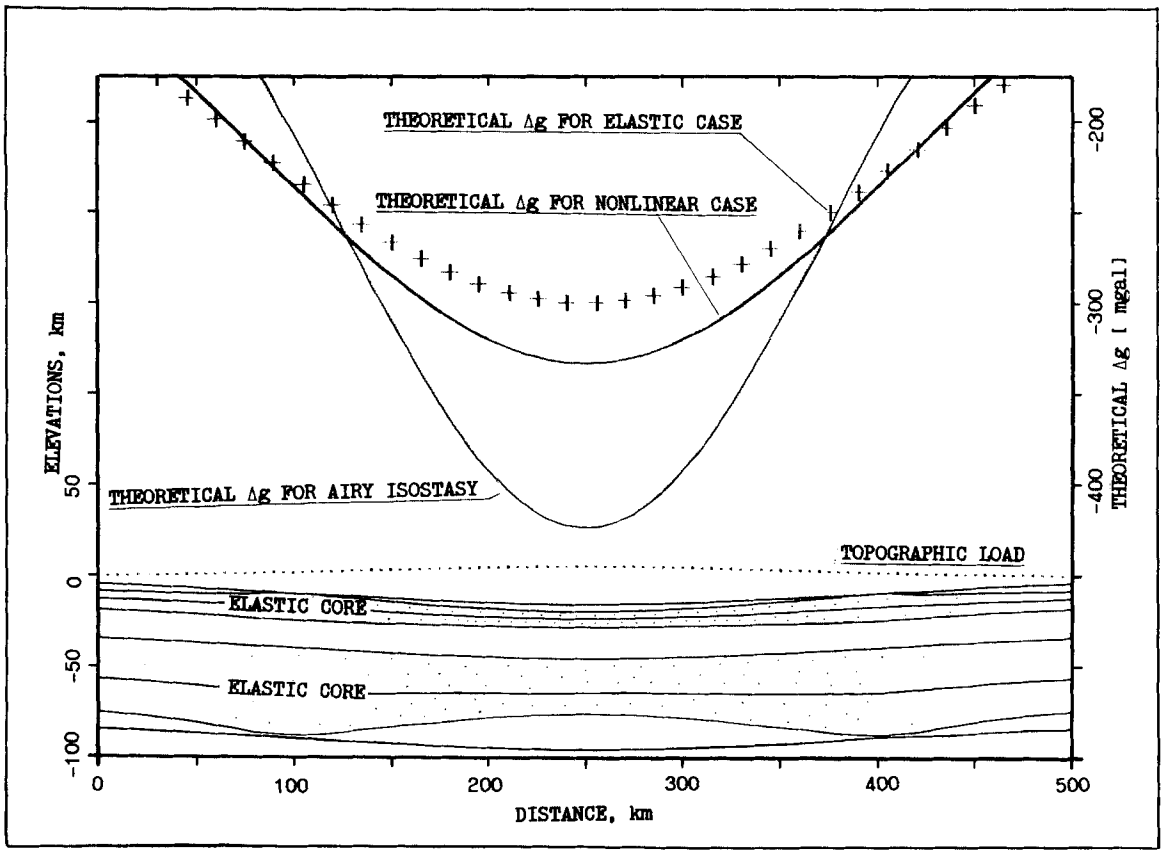

Figure 7. Influence of the distributed topographic load leads to a significant thinning of the plate. The plate beneath mountainous region may be weaker and therefore more 'locally compensated' than the adjacent region. The parameters used are the same as in Fig. 4. The plate is loaded by an symmetrical 'Gaussian' mountain 5 km in height, 100 km in radius. Broadest mountainous area can produce greater thinning. Theoretical gravity responses are computed for the non-linear case (thick solid line, $h_1 = 15$ km, $h = 30$ km, $h_2 = 80$), the purely elastic case (crosses, $h_e = [h_1^3 + (h_2 - h)^3]^{1/3} \approx 50$ km) and an Airy model (thin line).

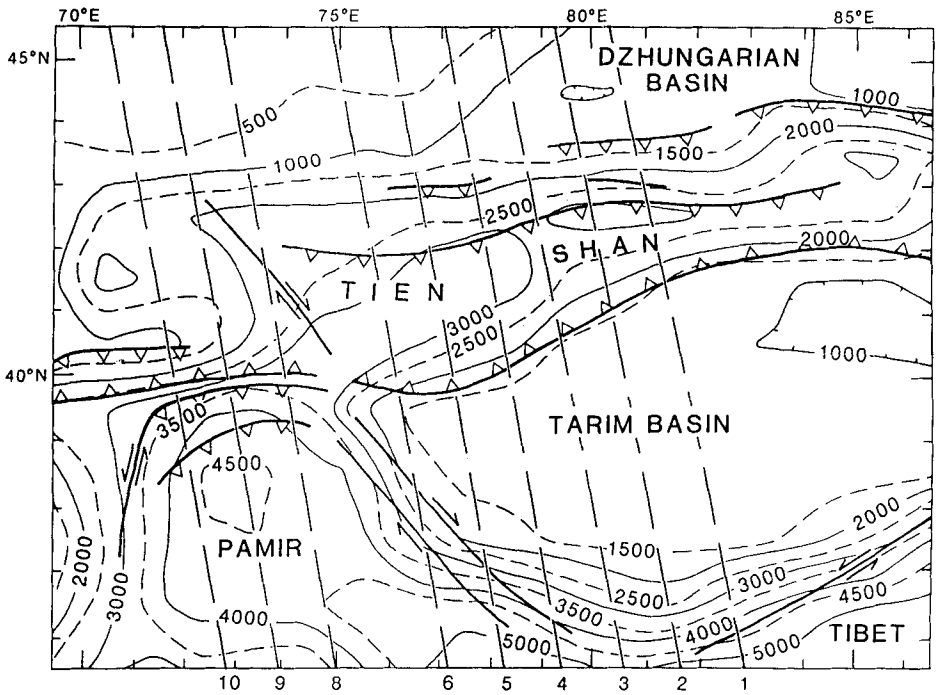

Figure 8. Map of mean elevations of the Tien Shan, Kazakh shield and Tarim Basin by Burov *et al.* (1990). The gravity data profiles are numbered as 1, 2, . . . , 10.

Downloaded from http://gji.oxfordjournals.org/ at UPMC on August 16, 2016

In the present study we show that deviations from elastic solutions may take place for areas with relatively intensive flexural deformations. Nevertheless, the deflections of interacting plates in the considered region are not too high and for this case there is no reason to expect large discrepancies between $w(x)$ obtained from the multilayered model and $w(x)$ obtained from a simple elastic approximation. This probably explains the fact that the elastic model provided here a satisfactory fit to the gravity data. However, due to its simplicity, the elastic model is unable to explain many aspects related to the internal structure of the lithosphere. In other words, it is difficult to associate the single output parameter of the elastic model—the equivalent (or effective) elastic thickness—with any level inside of the lithosphere or even to interpret the differentiation in effective rigidities. The values of flexural stresses prediced by the elastic model are also somewhat unrealistic in the light of mechanical properties of the rocks. Therefore, the main goal we followed here running more complicated numerical experiments for the Tien Shan was to try to detect and explain effects which are clearly beyond the scope of abilities of elastic modelling. In this case, using a more sophisticated model we do not intend to improve the fit to the data, but to get some additional information on the internal structure of the lithosphere (including stress distribution and the location of the rheological layers which allow us to predict the geometry and position of brittle seismogenic zones and zones of abnormal viscosity apparently correlating with anomalies of seismic velocities) and, furthermore, we can try to better understand the significance of the equivalent elastic thickness computed previously for various areas.

The data which we used for our computations were taken from Burov *et al.* (1990). To model the interaction of the Tarim block and Kazakh shield underthrusting flanks of the Tien Shan, we consider two separate semi-infinite plates underlying the areas north and south of the axis of the mountain region. The break is assumed to lie at the minima in the Bouguer anomaly (≈41°N–41.5°N for profile 2, Fig. 8). The southern Precambrian Tarim block corresponds to the parameters of the yield stress

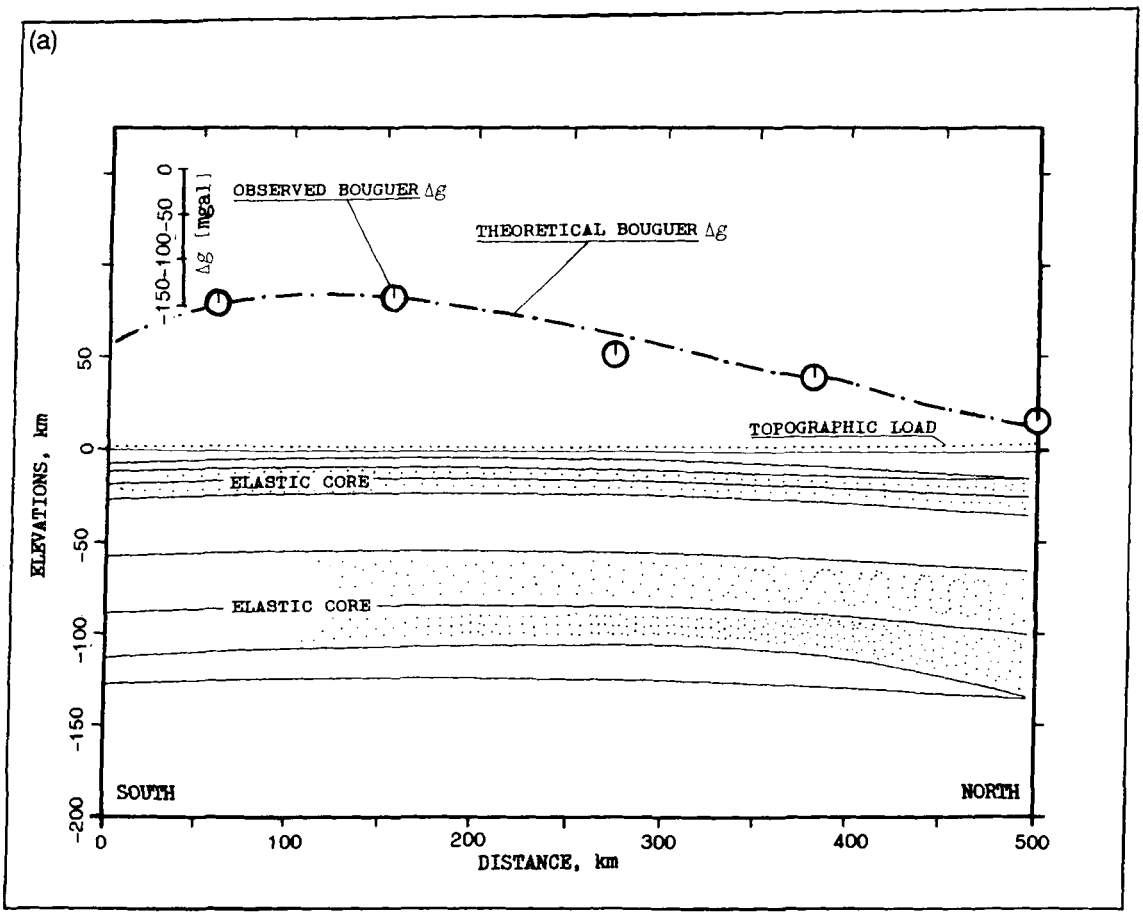

Figure 9. Application of our model to the case of Tarim basin. The topography and gravity data are taken from Burov *et al.* (1990), profile 2 in Fig. 8, part to the south of the Tien Shan. (a) Behaviour of Tarim block under the real topographic load. The boundary moment $M = 2.0 \times 10^{16}$ N m m^{-1} and force $F = 4.0 \times 10^{12}$ N m^{-1} are applied at the northern edge which subducts beneath the Tien Shan. Observed Bouguer gravity (circles) is compared with the theoretical gravity (dots) due to the deflection of the Moho zone. Sediment density used for the basin $\rho_s = 2600$ kg m^{-3}. Density used for other rocks above the Moho is $\rho_c = 2670$ kg m^{-3}. (b) The top figure shows the comparison of the observed Bouguer gravity anomalies (circles) over the Tarim basin with the theoretical anomalies produced by deflection of the plate using the multilayered model (curve 2) and assuming a purely elastic model with thickness $h_e = 50$ km (curve 1); 65 km (curve 3); 75 km (curve 4); and 100 km (curve 5) (Burov *et al.* 1990). The bottom figure shows the corresponding deflections. The non-elastic case fits the data better than the best solutions for the purely elastic cases.

Downloaded from http://gji.oxfordjournals.org/ at UPMC on August 16, 2016

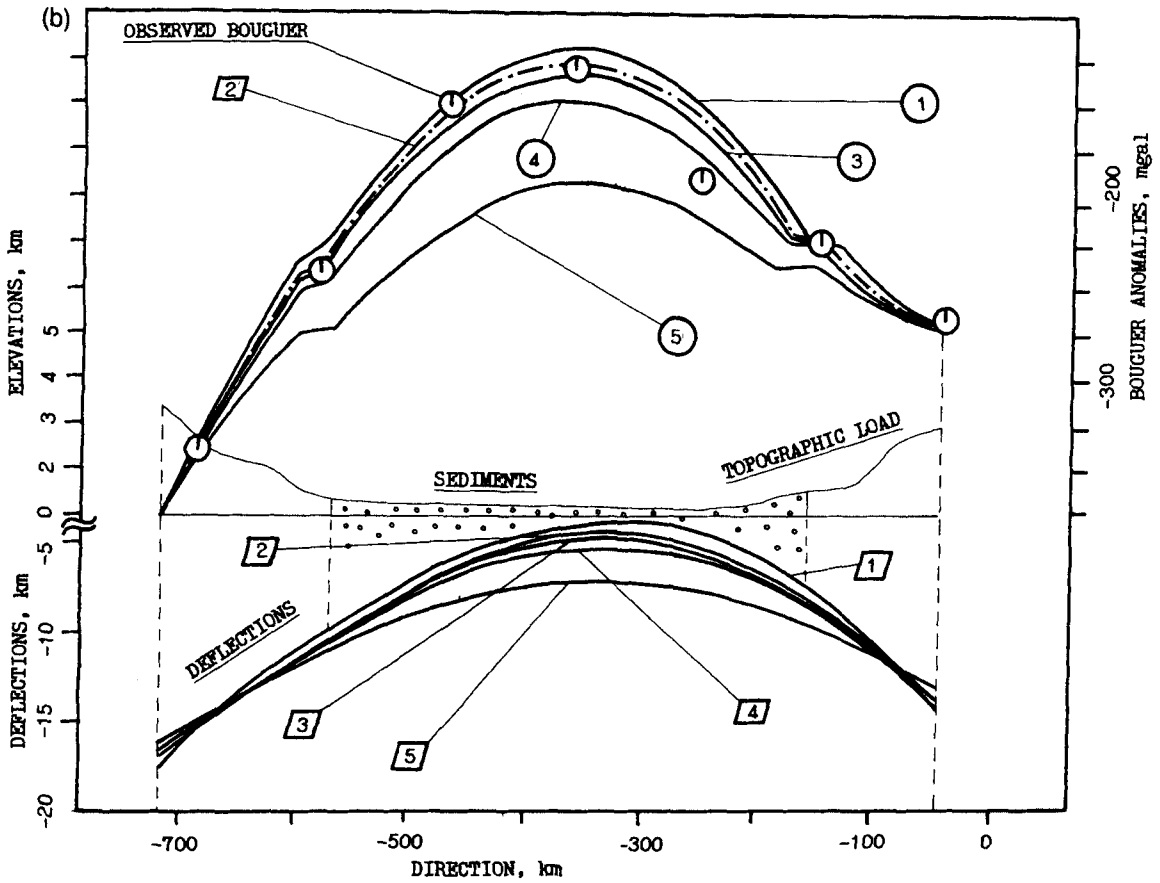

Figure 9 (*Continued*)

envelope from Fig. 2. It did not undergo any thermal rejuvenations (Molnar & Tapponnier 1978; Lyon-Caen & Molnar 1984) and we therefore assume that its geological age is the same as the thermal age.

The results for Tarim area are summarized in Fig. 9. These figures show a good agreement between the theoretical gravity signal due to the deflection of the plate beneath the Tarim basin and the observed Bouguer gravity anomalies [terrain corrections were applied to the data and a long-wavelength gravity field (first 10 harmonics, wavelength more than 4000 km) was also removed, see details in Burov *et al.* (1990)]. Fig. 9(b) also shows the match between the theoretical deflection produced by our multilayered model and that produced by the purely elastic models previously used in Burov *et al.* (1990). One can see that the curve for deflection in the non-elastic case lies somewhere between the best-fitting 'elastic' curves for 50 and 65 km thick plate. So the average 'equivalent' mechanical thickness of the non-elastic plate in the deformed area is less than $h_e = 70$ km that could be predicted from (12) for purely elastic continental plate. This discrepancy means that, even for relatively small flexure (as is the case in this area), the non-elastic behaviour plays a detectable role in shaping the Moho boundary. The location and shape of the brittle, elastic and ductile zones are also predicted. As the calculated elastic stresses due to the flexure in the case of Tarim block exceed the yield stress for brittle failure in the crustal part of the lithosphere but not in the mantle part, one can explain the presence of shallow earthquakes and the absence of deep ones. The predicted depths of the brittle zones (10–15 km for the Southern Tien Shan and 20–30 km for the Northern Tien Shan) are consistent with typical focal depths of earthquakes for this area [10–13 and 25–44 km respectively, by Nelson, McCaffrey & Molnar (1987)].

North of the Tarim block lies the Palaeozoic Kazakh shield which collides with the Tarim block beneath Tien Shan. Substitution of a geologic age of the shield into (6) yields a plate with an average elastic thickness of about 65 km. This estimate does not agree with the results of Burov *et al.* (1990) who found that an average elastic thickness of about 15–25 km provides the best fit to the Bouguer gravity data. The area probably underwent some kind of thermal rejuvenation in the Jurassic period (Babaev, Koshlakov & Mirzoev 1978). Using our non-linear model for a plate of such age (≈175 Myr), we obtain a depth to the mechanical bottom of 73–79 km and an effective variable elastic thickness of 15–25 km respectively (Fig. 10). The stresses caused by loading of the plate with the Tien Shan mountains contributed significantly to the thinning of the plate. We thus are able to explain why many continental plates have apparent effective rigidities much smaller than those predicted based on their geological ages. The general agreement between the results 'naturally' obtained on the basis of the thermal age and those obtained from the elastic model by fitting to the observational data is probably a strong arguement in

Downloaded from http://gji.oxfordjournals.org/ at UPMC on August 16, 2016

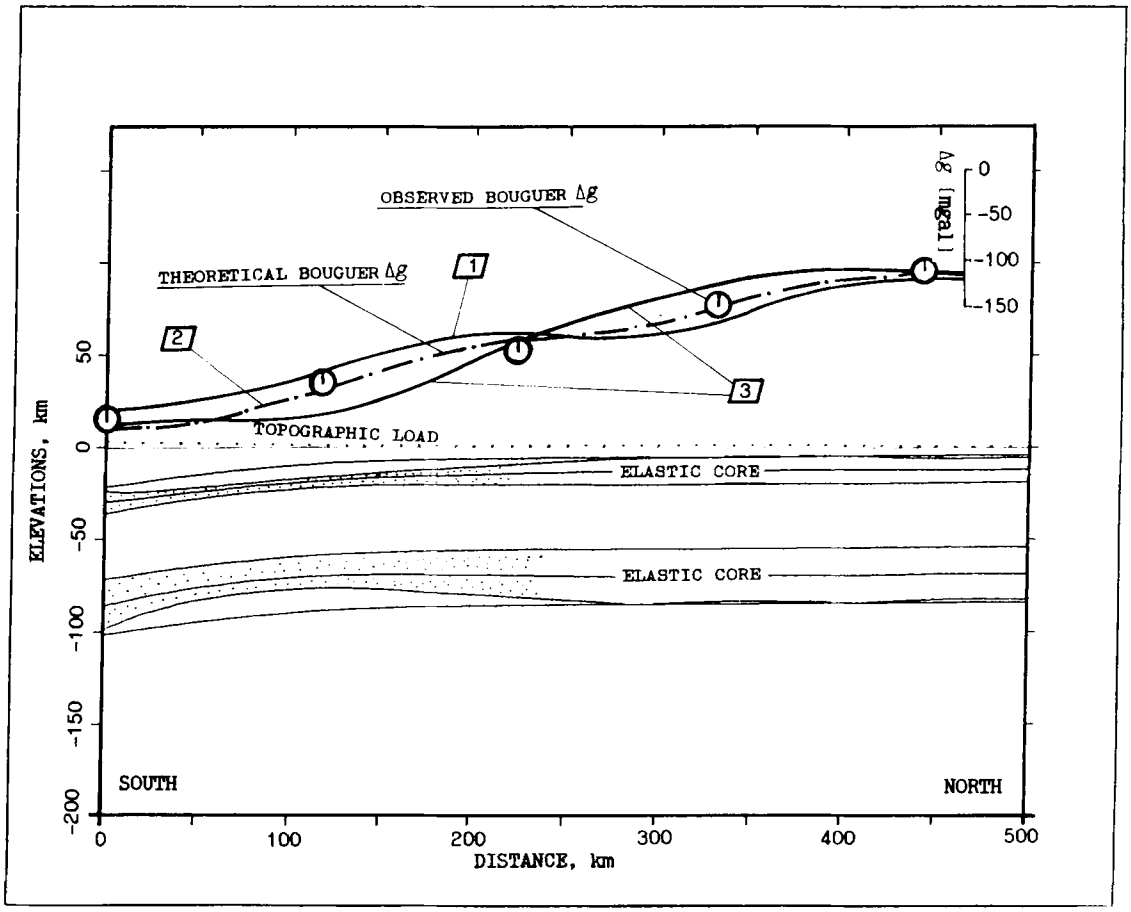

Figure 10. Application of the model to the case of thermally young Kazakh shield (the profile 2 in Fig. 8, part to the north of the Tien Shan). The computations are analogous to those of Fig. 8(a). Curve 1 corresponds to the theoretical gravity signal for the purely elastic plate with $h_e = 10$ km; curve 3 corresponds to that for $h_e = 25$ km. Curve 2 gives the solution for the multilayered model with the boundary moment $M = 2.0 \times 10^{16}$ N m m^{-1} and boundary force $F = 2.0 \times 10^{12}$ N m^{-1} applied to the southern edge of the Kazakh shield. The area probably underwent some thermal rejuvenation in Jurassic time. Solving the problem for a plate of Jurassic age (≈175 Ma), we obtain the depth to the mechanical bottom at 73–79 km and an average effective elastic thickness of about 25 km.

favour of using our approach for estimating the actual thermal age of the plate in the cases when introduction of the geological age fails to explain the data.

Finally, we have to note that the real behaviour of the lithosphere is more complicated than that described by our model. Such factors as fluids, pore pressure, semibrittle behaviour of rocks rather than an immediate brittle/ductile transition (Byerlee 1978), time-dependent influence of loads, different chemical processes, and viscous flow in a lower crust probably are able to significantly affect the shape of the resulting yield envelope (Kirby 1987). Influence of lithospheric rocks (like diabase), with properties somewhat different from quartz and olivine is also highly important and can produce additional weak places in the envelope (Shudofsky *et al.* 1987). Moreover, from one side one should note that computations were additionally simplified by ignoring the lateral variations in rheology while the response of many areas may be strongly controlled by these heterogeneities. But from the other side the information on such variations, except some well-studied cases like the Pyrenees, is usually indirect and not reliable enough for immediate use in the model. Nevertheless, the model used here incorporates the most important rheological features of the continental lithosphere and should therefore serve as a basis for further investigations of effects related to flexure of lithosphere.

ACKNOWLEDGMENTS

We thank M. Kogan, H. Lyon-Caen, M. McNutt, P. Molnar, C. Ruppel, P. Tapponnier and L. Lobkovsky for critical readings and helpful discussions. We appreciated the comments of two anonymous reviewers. This study was carried out in the framework of the CNRS (France)–Academy of Sciences (USSR) cooperation agreement.

Downloaded from http://gji.oxfordjournals.org/ at UPMC on August 16, 2016

REFERENCES

Babaev, A. M., Koshlakov, G. V. & Mirzoev, K. M., 1978. *Seismic Regionalization of Tadjikistan,* Donish, Dushanbe (in Russian).

Brace, W. F. & Kohlstedt, D. L., 1980. Limits on lithospheric stress imposed by laboratory experiments, *J. geophys. Res.*, **85,** 6248–6252.

Burov, E. B. & Kogan, M. G., 1990. Gravitational–mechanical model of the continental plate collision in the Tien Shan region, *Dok. Acad. Nauk, Phys. Solid Earth,* **313,** 1439–1444 (in Russian).

Burov, E. B., Kogan, M. G., Lyon-Caen, H. & Molnar, P., 1990. Gravity anomalies, the deep structure, and dynamic processes beneath the Tien Shan, *Earth planet. Sci. Lett.*, **96,** 367–383.

Byerlee, J. D., 1968. Brittle–ductile transition in rocks, *J. Geophys. Res.*, **73,** 4741–4750.

Byerlee, J. D., 1978. Friction of rocks, *Pure appl. Geophys,* **116,** 615–626.

Carslaw, H. S. & Jaeger, J. C., 1964. *Conduction of Heat in Solids,* Clarendon Press, Oxford (Russian translation: Nauka, Moscow).

Chamot-Rooke, N. & Le Pichon, X., 1989. Zenisu Ridge: mechanical model of formation, *Tectonophysics,* **160,** 175–193.

Chen, W. P. & Molnar, P., 1983. Focal depths of intracontinental earthquakes and their implications for the thermal and mechanical properties of the lithosphere, *J. geophys. Res.*, **88,** 4183–4214.

De Bremaecker, J. C., 1977. Is the oceanic lithosphere elastic or viscous? *J. geophys. Res.*, **82,** 2001–2004.

De Rito, R. F., Lachenbruch, A. H., Moses, T. H. Jr & Munro, R. J., 1989. Heat flow and thermotectonic problems of the Central Ventura Basin, Southern California, *J. geophys. Res.*, **94,** 681–699.

Dorman, L. M. & Lewis, B. T. R., 1972. Correlation of Bouguer gravity anomalies with topography for the United States, *J. geophys. Res.*, **77,** 3068–3077.

Dubois, J., Launay, J., Recy, J. & Marshall, J., 1977. New Hebrides trench: subduction rate from associated lithospheric bulge, *Canadian J. Earth Sci.*, **14,** 250–255.

Goetze, C. & Evans, B., 1979. Stress and temperature in the bending lithosphere as constrained by experimental rock mechanics, *Geophys. J. R. astr. Soc.*, **59,** 463–478.

Karner, G. & Watts, A. B., 1983. Gravity anomalies and flexure of the lithosphere at mountain ranges, *J. geophys. Res.*, **88,** 10 449–10 477.

Keller, H. B., 1974. Accurate difference methods for non-linear two-point boundary problems, *SIAM J. Numer. Anal.*, **11,** 305–320.

Kirby, S. H., 1983. Rheology of the lithosphere, *Rev. Geophys.*, **21,** 1458–1487.

Kirby, S. H., 1985. Rock mechanics observations pertinent to the rheology of the continental lithosphere and the localization of strain along shear zones, *Tectonophysics,* **119,** 1–27.

Kirby, S. H. & Kronenberg, A. K., 1987. Rheology of the lithosphere: selected topics, *Rev. Geophys.*, **25,** 1219–1244.

Koch, P. S., Christie, J. M., Ord, A. & George, R. R., 1989. Effect of water on the rheology of experimentally deformed quartzite, *J. geophys. Res.*, **94,** 13 975–13 996.

Kusznir, N. & Karner, G., 1985. Dependence or the flexural rigidity of the continental lithosphere on rheology and temperature, *Nature,* **316,** 138–142.

Lerner-Lam, A. L. & Jordan, T. H., 1987. How thick are the continents? *J. geophys. Res.*, **92,** 14 007–14 026.

Lyon-Caen, H. & Molnar, P., 1983. Constraints on the structure of the Himalaya from an analysis of gravity anomalies and a flexural model of the lithosphere, *J. geophys. Res.*, **88,** 8171–8191.

Lyon-Caen, H. & Molnar, P., 1984. Gravity anomalies of the western Tibet and the southern Tarim basin, *Geophys. Res. Lett.*, **11,** 1251–1254.

Mackwell, S. J., Bai, Q. & Kohlstedt, D. L., 1990. Rheology of olivine and the strength of the lithosphere, *Geophys. Res. Lett.*, **17,** 9–12.

McAdoo, D. C., Caldwell, J. G. & Turcotte, D. L., 1978. On the elastic-perfectly plastic bending of the lithosphere under generalized loading with application to the Kurile Trench, *Geophys. J. R. astr. Soc.*, **54,** 11–26.

McAdoo, D. C. & Sandwell, D., 1985. Folding of oceanic lithosphere, *J. geophys. Res.*, **90,** 8563–8569.

McAdoo, D. C., Martin, C. F. & Polouse, S., 1985. Seasat observations of flexure: evidence for a strong lithosphere, *Tectonophysics,* **116,** 209–222.

McNutt, M., 1980. Implications of regional gravity for state of stress in the Earth's crust and upper mantle, *J. geophys. Res.*, **85,** 6377–6396.

McNutt, M. & Menard, H. W., 1982. Constraints on the yield strength in the oceanic lithosphere derived from observations of flexure, *Geophys. J. R. astr. Soc.*, **59,** 4663–478.

McNutt, M., Diament, M. & Kogan, M. G., 1988. Variations of elastic plate thickness at continental thrust belts, *J. geophys. Res.*, **93,** 8825–8838.

Meissner, R. & Strehlau, J., 1982. Limits of stresses in continental crusts and their relation to the depth–frequency distribution of shallow earthquakes, *Tectonics,* **1,** 73–89.

Melosh, H. J., 1978. Dynamic support of the outer rise, *Geophys. Res. Lett.*, **5,** 321–324.

Molnar, P. & Tapponnier, P., 1978. Active tectonics of Tibet, *J. geophys. Res.*, **83,** 5361–5375.

Molnar, P. & Tapponnier, P., 1981. A possible dependence of tectonic strength on the age of the crust in Asia, *Earth planet. Sci. Lett.*, **52,** 107–114.

Na, T. Y., 1979. *Computational Methods in Engineering Boundary Value Problems,* Academic Press, New York, 309 pp.

Nelson, M. R., McCaffrey, R. & Molnar, P., 1987. Source parameters for 11 earthquakes in the Tien Shan, Central Asia, determined by P and SH waveform inversion, *J. geophys. Res.*, **92,** 12 629–12 648.

Parsons, B. & Sclater, J. G., 1977. An analysis of the thermal structure of the plates, *J. geophys. Res.*, **82,** 803–827.

Ranalli, G. & Murphy, D. C., 1987. Rheological stratification of the lithosphere, *Tectonophysics,* **132,** 281–295.

Sclater, J. G., Jaupart, C. & Galson, D., 1980. The heat flow through oceanic and continental crust and the heat loss of the Earth, *Rev. Geophys. Space Phys.*, **18,** 269–311.

Shudovsky, G. N., Cloetingh, S., Stein, S. & Wortel, R., 1987. Unusually deep earthquakes in East Africa: constraints on the thermomechanical structure of a continental rift system, *Geophys. Res. Lett.*, **14,** 741–744.

Talwani, M., Worzel, J. L. & Landisman, M., 1959. Rapid gravity computation of two dimensional bodies with application to the Mendocino submarine fracture zone, *J. geophys. Res.*, **64,** 49–59.

Tsenn, M. C. & Carter, N. L., 1987. Flow properties of continental lithosphere, *Tectonophysics,* **136,** 27–63.

Turcotte, D. L., 1979. Flexure, in *Advances in Geophysics,* vol. 21, pp. 51–86, Academic Press, New York.

Turcotte, D. L. & Schubert, G., 1982. *Geodynamics Applications of Continuum Physics to Geological Problems,* Wiley, New York, 450 pp.

Watts, A. B. & Talwani, M., 1974. Gravity anomalies seaward of deep-sea trenches and their tectonic implications, *Geophys. J. R. astr. Soc.*, **36,** 57–90.

Downloaded from http://gji.oxfordjournals.org/ at UPMC on August 16, 2016

Zoback, M. D., Prescott, W. H. & Krueger, S. W. 1985. Evidence for lower crustal strain localization in elastic thickness of continental thrust belts, *Nature*, **317**, 7705–7707.

APPENDIX A

The accurate analytical solution of the heat-transfer equation for the continental lithosphere

Assuming that for the old continental plate the dependence of the temperature on the plate velocity can be neglected, we can obtain the temperature distribution $T = T(y)$ in the plate by solving the following system:

$$\begin{aligned} &\frac{1}{k_c}\frac{\partial T}{\partial t} - \frac{\partial^2 T}{\partial y^2} = \frac{\mu v_0^2/h^2}{k_c} + \frac{\rho_c H_s \exp\left(\frac{-h}{h_r}\right)}{k_c} && \text{for } y \leq h, \\ &\frac{1}{k_m}\frac{\partial T}{\partial t} - \frac{\partial^2 T}{\partial y^2} = 0 && \text{for } y > h. \end{aligned} \tag{A1}$$

The boundary and initial conditions are

$T(0, t) = 0$ (temperature at the upper surface = *const* = 0 °C),

$T(a, t) = T_m$ (temperature at the bottom = *const* = T_m),

$T(y, 0) = T_m$ (homogeneous temperature distribution at the beginning).

The term $\mu v_0^2/(h^2 k_c)$ is included to account for dissipative heat generation due to possible viscous sliding between the crustal and mantle portions of the lithosphere: μ is the mean viscosity of crustal material in the viscous channel, and v_0 is the mean velocity of relative sliding. In the present study we assume that no sliding occurs ($v_0 = 0$).

The homogeneous solution T_h of (A1) (Carslaw & Jaeger 1964) is

$$T_h(y, t) = T_m\left(\frac{y}{a} + \sum_{n=1} A_n \exp\left(-n^2\pi^2\chi t/a^2\right) \sin n\pi y/a\right).$$

The partial solution T_p of (A1) is obtained from the assumption that $T|_{h-0} = T|_{h+0}$ and $dT/dy|_{h-0} = dT/dy|_{h+0}$:

$$T_p = \begin{cases} T_{-p} = T_r + T_d & \text{for } y \leq h \\ T_{+p} = D_0 + D_1 y & \text{for } y > h \end{cases}$$

$$T_r = C_{r0} + C_{r1} y + \frac{\rho_c H_s h_r^2}{k}[1 - \exp(-y/h_r)], \qquad T_d = C_{d0} + C_{d1} y - \frac{\mu v_0^2 y^2}{2kh^2}, \qquad A_d = \mu v_0^2/h^2, \qquad A_r = \rho_c H_s h_r^2,$$

$$T_p = T_{-p}(y) = C_0 + C_1 y - A_d y^2/(2k) + (A_r/k)[1 - \exp(-y/h_r)] \quad \text{for } y \leq h$$

$$C_0 = C_{r0} = C_{d0} = 0, \qquad D_0 = -D_1 a,$$

$$T_p = T_{+p}(y) = D_1(y - a), \qquad \text{for } y > h$$

General solution in dimensionless variables $\tilde{h} = h/a$, $\tilde{y} = y/a$, $\tilde{t} = t\chi/(a^2)$

$$T(\tilde{y}, \tilde{t}) = T_p + T_m\left(\tilde{y} + \sum_{n=1}^{\infty} A_n \exp\left(-n^2\pi^2\tilde{t}\right) \sin\left(n\pi\tilde{y}\right)\right),$$

$$T_p = \begin{cases} a\tilde{C}_1\tilde{y} - \dfrac{A_d a^2 \tilde{y}^2}{2k} + \dfrac{A_r}{k}[1 - \exp(-a\tilde{y}/h_r)] & \text{for } \tilde{y} \leq \tilde{h}, \\ a\tilde{D}_1(\tilde{y} - 1) & \text{for } \tilde{y} > \tilde{h}, \end{cases}$$

$$C_1 = \tilde{C}_1 = \frac{A_d h}{2ak}(2a - h) + \frac{A_r}{ak}\left[\frac{\exp(-h/h_r)}{h_r}(h + h_r - a) - 1\right], \qquad D_1 = \tilde{D}_1 = -\frac{A_d h^2}{2ak}$$

$$+ \frac{A_r}{ak}\left[\frac{\exp(-h/h_r)}{h_r}(h + h_r) - 1\right], \qquad A_n = \frac{2}{\pi n} - \frac{2}{T_m} - \frac{2}{T_m}\sum_{i=1}^{4}\int_i,$$

where

$$\int_1 = \tilde{C}_1 a\left[\frac{\sin n\pi\tilde{h}}{(n\pi)^2} - \frac{\tilde{h}}{n\pi}\cos n\pi\tilde{h}\right], \qquad \int_2 = -\frac{a^2 A_d}{k}\left[\frac{2\tilde{h}\sin(n\pi\tilde{h})}{(n\pi)^2} - \frac{(n^2\pi^2\tilde{h}^2 - 2)}{(n\pi)^3}\cos(n\pi\tilde{h}) + \frac{2}{(n\pi)^3}\right],$$

$$\int_3 = \frac{A_r}{k}\left[-\frac{1}{n\pi}\cos(n\pi\tilde{h}) + 1 + \exp\left(\frac{-\tilde{h}a}{h_r}\right)\frac{\left[\left(\frac{-a}{h_r}\right)\sin n\pi\tilde{h} - n\pi\cos n\pi\tilde{h}\right] + n\pi}{\tilde{h}^{-2} + (n\pi)^2}\right],$$

$$\int_4 = a\tilde{D}_1\left[-1/(n\pi)^2 \sin n\pi\tilde{h} + \frac{\cos n\pi\tilde{h}}{n\pi}(\tilde{h} - 1)\right].$$

Downloaded from http://gji.oxfordjournals.org/ at UPMC on August 16, 2016